Atmos. Chem. Phys. Discuss., https://doi.org/10.5194/acp-2019-192
Manuscript under review for journal Atmos. Chem. Phys.
Discussion started: 12 March 2019

Atmospheric Chemistry and Physics Discussions

Summertime surface PM_1 aerosol composition and size by source region at the Lampedusa island in the central Mediterranean Sea

Marc D. Mallet[1,2,3], Barbara D'Anna[2,4], Aurélie Même[2,*], Maria Chiara Bove[5,6], Federico Cassola[5,7], Giandomenico Pace[8], Karine Desboeufs[1], Claudia Di Biagio[1], Jean-Francois Doussin[1], Michel Maille[1], Dario Massabò[5], Jean Sciare[9], Pascal Zapf[1], Alcide Giorgio di Sarra[8] and Paola Formenti[1]

1. LISA, CNRS UMR7583, Université Paris Est Créteil (UPEC), Université Paris Diderot (UPD), Institut Pierre Simon Laplace (IPSL), Créteil, France
2. IRCELYON, CNRS UMR 5652, Univ. Lyon1, Lyon, France
3. Centre National d'Etudes Spatiales (CNES), Toulouse, France
4. LCE, CNRS UMR 7376, Aix-Marseille Université, Marseille, France
5. Department of Physics & INFN, University of Genoa, Genoa, Italy
6. ARPAL Physical Agents and Air Pollution Sector, La Spezia, Italy
7. ARPAL CFMI-PC, Genoa, Italy (current affiliation)
8. Laboratory for Observations and Analyses of Earth and Climate, ENEA, Rome, Italy
9. The Cyprus Institute, Energy, Environment and Water Research Center, Nicosia, Cyprus

* now at Bruker

Abstract

Measurements of aerosol composition and size distributions were taken during the summer of 2013 at the remote island of Lampedusa in the southern central Mediterranean Sea. These measurements were part of the ChArMEx/ADRIMED (Chemistry and Aerosol Mediterranean Experiment/Aerosol Direct Radiative Forcing on the Mediterranean Climate) framework and took place during the Special Observation Period 1a (SOP-1a) from 11 June until 5 July 2013.

From compact time-of-flight aerosol mass spectrometer (cToF-AMS) measurements in the size range below 1 µm in aerodynamic diameter (PM_1), particles were predominately comprised of ammonium and sulphate. On average, ammonium sulphate contributed 63% to the non-refractory PM_1 mass, followed by organics (33%). The organic aerosol was generally

very highly oxidised (f_{44} values were typically between 0.25 and 0.26). The contribution of ammonium sulphate was generally higher than organic aerosol in comparison to measurements taken in the western Mediterranean but is consistent with studies undertaken in the eastern basin.

Source apportionment of organics using a statistical (positive matrix factorisation) model revealed four factors; a hydrocarbon-like organic aerosol (HOA), a methanesulfonic acid related oxygenated organic aerosol (MSA-OOA), a more oxidised oxygenated organic aerosol (MO-OOA) and a less oxidised oxygenated organic aerosol we label (LO-OOA). The MO-OOA was the dominant factor for most of the campaign (53% of the PM_1 OA mass). It was well correlated with SO_4^{2-}, highly oxidised, and generally more dominant during easterly air masses originating from the eastern Mediterranean and central Europe. The LO-OOA factor had a very similar composition to the MO-OOA factor, but was more prevalent during westerly winds with air masses originating from the Atlantic Ocean, the western Mediterranean, and in high altitudes over France and Spain from mistral winds. The MSA-OOA factor contributed an average 12% to the PM_1 OA and was more dominant during the mistral winds. The HOA, representing observed primary organic aerosol only contributed 8% of the average PM_1 OA during the campaign.

Even though Lampedusa is one of the most remote sites in the Mediterranean, PM_1 concentrations (10 ± 5 μg m^{-3}) were comparable to those observed in coastal cities and sites closer to continental Europe. Cleaner conditions corresponded to higher wind speeds. Nucleation and growth of new aerosol particles was observed during periods of northwesterly winds. From a climatology analysis from 1999 until 2012, these periods were much more prevalent during the measurement campaign than during the preceding 13 years. These results support previous findings that highlight the importance of different large-scale synoptic conditions in determining the regional and local aerosol composition and oxidation and also suggest that a non-polluted surface atmosphere over the Mediterranean is rare.

1. Introduction

The Mediterranean Sea is a unique marine environment, surrounded by mountain ranges and high coastal human populations from Africa, Europe, and Asia, and the two largest deserts in the world; Sahara Desert to the south and Arabian Desert to the East. It presents a diverse

and dynamic atmospheric composition and is projected to undergo significant changes in the contribution of freshwater (Sanchez-Gomez et al., 2009), sea surface temperature and precipitation (Mariotti et al., 2015) over the coming decades. The burning of fossil fuels, including shipping pollution, in southern Europe and in large Mediterranean cities, as well as natural sources of aerosol such as sea salt, forest fires and mineral dust provide a highly complex and dynamic mixture of organic and inorganic aerosol and aerosol precursors in this region (Lelieveld et al., 2002). Elevated aerosol loadings over the Mediterranean basin have been attributed to the long-range transport of continental anthropogenic aerosols (Perrone et al., 2013; Sciare et al., 2003; Sciare et al., 2008) and mineral dust transported from Africa (Querol et al., 2009b; Koçak et al., 2007). Boundary layer observations in the eastern Mediterranean have shown significant influence of long-range transported continental pollution from southern and central Europe (Sciare et al., 2003). Furthermore, biomass burning aerosol has frequently been observed over the basin, in particular the dry season in summer when forest fires are more common (Pace et al., 2005). Long-ranged plumes from north American fires have also been observed at high altitudes (Formenti et al., 2002; Ortiz-Amezcua et al., 2014; Brocchi et al., 2018; Ancellet et al., 2016).

Previous long-term observations of the chemical composition of aerosol in the Mediterranean have shown that PM_{10} (particulate mass with aerodynamic diameter less than 10 µm) is composed of secondary ammonium sulphate, primary and secondary organic aerosol from fossil fuels or biogenic origins, with contributions from natural aerosols from the Sahara Desert and sea spray (Bove et al., 2016; Koulouri et al., 2008; Schembari et al., 2014; Calzolai et al., 2015). Mineral and sea salt contributions are significantly less in $PM_{2.5}$ particle fraction (Querol et al., 2009a). Coarse mode particles contribute to the direct radiative effect over the Mediterranean (Perrone and Bergamo, 2011; Meloni et al., 2006) and can also act as condensation sinks for pollutants (Pikridas et al., 2012). Smaller (sub-micron) aerosol particles, while also contributing efficiently to the total aerosol optical depth in this region (Formenti et al., 2018), can also act as efficient cloud condensation nuclei and therefore have influence on cloud formation, lifetime and precipitation (Haywood and Boucher, 2000). Understanding the impact of different natural and anthropogenic sources on the regional composition of the atmosphere is therefore important in our understanding of the influences they have on the climate over the Mediterranean basin and surrounding regions. It is also

94 now widely recognised that aerosols contribute to adverse health effects in humans (World
95 Health Organization, 2016).

96 Consideration of both the local and regional meteorology are needed to characterise the
97 sources and aging of aerosols (Petit et al., 2017). The National Oceanic and Atmospheric
98 Administration's (NOAA) Hybrid Single-Particle Lagrangian Integrated Trajectory model
99 (HYSPLIT; Stein et al., 2015) and other trajectory models (e.g. FLEXPART; (Stohl et al., 2005)
100 have become a widely-used resources in atmospheric studies to compute the backwards or
101 forwards trajectories of air masses at any point on Earth. They can be useful for identifying
102 the possible origin of a particular episode associated with elevated concentrations of aerosols
103 or gases. Combined with in-situ measurements over longer time periods, they provide a more
104 holistic approach in understanding the link between local or region meteorology and
105 atmospheric composition (Schmale et al., 2013; Tadros et al., 2018; Zhou et al., 2016). This is
106 particularly useful for remote sites where local emissions are insignificant or infrequent.

107 Investigation of the aerosol physical and chemical properties can also help distinguish their
108 respective sources. Positive matrix factorisation (PMF; (Paatero, 1997; Paatero and Tapper,
109 1994) has proved to be a useful statistical tool in identifying aerosol sources or aging
110 processes of organics. The source apportionment of $PM_{2.5}$ and PM_{10} over the Mediterranean,
111 from PMF method, has been investigated in recent works and showed a large spatial
112 variability in source contributions (Becagli et al., 2012; 2017; Calzolai et al., 2015; Amato et
113 al., 2016; Diapouli et al., 2017). The PMF approach was also used to study the aerosol source
114 and aging processes by utilising the complex nature of organic aerosol in the Mediterranean
115 (e.g. Hildebrandt et al., 2010, 2011; Bougiatioti et al., 2014; Minguillón et al., 2016; Arndt et
116 al., 2017; Michoud et al., 2017). This approach has become increasingly feasible with the
117 recent widespread implementation of instruments capable of providing real-time, high time-
118 and mass-resolved non-refractory aerosol composition, such as aerosol mass spectrometers
119 (Ulbrich et al., 2009). PMF models have shown to successfully resolve the bulk-composition
120 of sub-micron organic aerosol into the contributions from various primary sources (e.g.
121 biomass burning, fossil fuel burning, cooking aerosol), but can also reveal the contributions
122 and characteristics of secondary (SOA) organic aerosol (Zhang et al., 2011). Factors with
123 similar mass spectra are consistently observed, albeit with different contributions at
124 measuring sites all around the world. The most commonly observed primary organic aerosol

125 factors are hydrocarbon-like OA (HOA), usually from fossil fuel burning as well as biomass
126 burning (BBA) while SOA can be usually separated into at least two factors, with low-volatility
127 oxygenated OA (LV-OOA) and Semi-Volatile-OOA (SV-OOA) as common examples (Zhang et
128 al., 2011; Crippa et al., 2014). Other types of OOA have also been observed, such as "Marine-
129 OOA" (Schmale et al., 2013), although these are more difficult to resolve given the shift
130 towards more uniform OA composition with aging.

131 The Chemistry-Aerosol Mediterranean Experiment (ChArMEx) collaborative research
132 program, and the Aerosol Direct Radiative Impact on the regional climate in the
133 MEDiterranean region (ADRIMED) project within, were undertaken to investigate the
134 chemistry and climate interactions within the Mediterranean (Mallet et al., 2016). From 11
135 June until 5 July 2013, numerous experimental setups were deployed across the western and
136 central Mediterranean in what is called the "Special Observation Period - 1a" (SOP-1a),
137 including intensive airborne measurements (Denjean et al., 2016). Two super-sites were set-
138 up at Ersa (at the northern tip of Corsica Island, France) and at the Lampedusa Island (Italy),
139 approximately 1000 km apart on a north-to-south axis in order to characterise surface aerosol
140 chemical, physical and optical properties (Mallet et al., 2016). Numerous secondary sites were
141 established along the Mediterranean coasts in Spain, Italy and Corsica beyond the SOP-1a
142 have also provided valuable knowledge of the atmospheric composition in the western and
143 central Mediterranean regions (Chrit et al., 2017; Chrit et al., 2018; Becagli et al., 2017).

144 In this paper, we present the first detailed characterisation of PM_1 in the central
145 Mediterranean region from measurements of size-resolved chemical composition from the
146 island site of Lampedusa during the ChArMex/ADRIMED SOP-1a. We investigate the source
147 apportionment of PM_1 by considering their chemical and microphysical properties along with
148 ancillary PM_{10}, gaseous and meteorological data, air mass back trajectories as well as
149 complimentary data collected at the Ersa site in Corsica.

150 2. Experimental

151 2.1 Sampling sites

152 Observations took place at the Roberto Serao station on the island of Lampedusa (35°31'5''N,
153 12°37'51'' E, 20 m above sea level) from 11 June to 5 July 2013. Ancillary measurements for

this study taken at Ersa at the northern tip of Cape Corsica (42°58'5" N, 9°22'49" E, 560 m above sea level), are also considered. The position of the stations is shown in Figure 1.

2.2 Instrumentation, measurements and data

Instruments at the Lampedusa super-site were housed in the PEGASUS (Portable Gas Field and Aerosol Sampling Unit) station, a portable observatory initiated by LISA, described in Mallet et al. (2016). Relevant to this study, a c-ToF-AMS (Aerodyne Inc., Billerica, USA), was used to measure the size-resolved composition of non-refractory particulate matter below 1 µm (NF-PM_1)(Drewnick et al., 2005). Data was collected with a 3-minute time resolution. The c-ToF-AMS was operated from a certified Total Suspected Particulate (TPS) sampling head (Rupprecht and Patashnick, Albany, NY, USA) followed by a cyclone impactor cutting off aerosol particles larger than 1 µm in aerodynamic diameter.

A particle-into-liquid sampler (Metrohm PILS; Orsini et al. (2003)) was installed on a TSP inlet and collected samples approximately every hour. Denuders to remove acid/base gases were not used. Samples were analysed for major and organic anions (F^-, Cl^-, NO_3^-, SO_4^{2-}, PO_4^{3-}, $HCOO^-$, CH_3COO^-, $(COO^-)_2$) and cations (Na^+, NH_4^+, K^+, Ca^{2+}, Mg^{2+}) using Ion Chromatography (Metrohm, model 850 Professional IC) equipped with Metrosep A supp 7 pre-column and column for anions measurements and Metrosep C4-250 mm pre-column and column for cations measurements, and a 500 µL injection loop. The device was operated with a 1-hour time resolution.

A 13-stage rotating cascade impactor nanoMOUDI (Model 125B, Marple et al., 1991) was used to measure the size-segregated inorganic elemental composition. The nanoMoudi impactor, also operated from the TSP inlet, allows the separation of the particles in 13 size classes from 10 nm to 10 µm diameter with a backup stage. Each sample was collected for 3 days to ensure enough material was collected on each impactor stage. Filters were then analysed using X-ray fluorescence (PW-2404 spectrometer by PANalytical™) for the particulate elemental concentrations for elements from Na to Pb as described in Denjean et al. (2016))

A Scanning Mobility Particle Sizer (SMPS) measured the mobility number size distribution of aerosols every 3 minutes from 14.6 to 661.2 nm. diameter. The instrument is composed by an X-ray electrostatic classifier (TSI Inc., model 3080) and a differential Mobility Analyser (DMA; TSI Inc., model 3081), and a condensation particle counter (CPC; TSI Inc., model 3775)

operated at 1.5/0.3 L min^{-1} aerosol/sheath flows. Data were corrected to take into account the particle electrical charging probabilities, the CPC counting efficiency, and diffusion losses. Each scan was recorded with a 5-minute time resolution. A drier was not used on the SMPS inlet and therefore the size distributions reported are for ambient conditions.

A GRIMM optical particle counter (OPC; GRIMM Inc., model 1.109) was used to measure the number size distribution over 31 size classes ranging from 0.26 µm up to 32 µm (nominal diameter range assuming the aerosol refractive index of latex spheres in the calibration protocol). The instrument was operated at a 6-second resolution and data were acquired as 3-minute averages.

The equivalent black carbon mass concentration (eBC) was determined by the measurement of light-attenuation at 880 nm performed by a spectral aethalometer (Magee Sci. model AE31) operated at a 2-minute time resolution and equipped with a TSP particle inlet. As the evaluation of eBC is used as a qualitative tracer of pollution, the factory mass conversion factor of 16.6 m^2 g^{-1} was applied to the raw measurement of attenuation without further corrections.

The meteorological measurements (air pressure, temperature, relative humidity, wind direction and speed and precipitation) were collected by a Vaisala Milos 500 station with a sampling rate of 10 minutes. The wind sensor was installed on a 10-m meteorological tower, while the air temperature and humidity were measured at a height of 2 m.

2.3. Data analysis

2.3.1. Analysis of the cToF-AMS data

The cToF-AMS data set was processed using two different software analysis tools. The first makes use of the widely-used and standard Igor Pro package, Squirrel (version 1.57G). This software processes the raw data and analyzes the unit-mass resolution (UMR) output with a fragmentation table reported in Aiken et al. (2008). The second method uses a cumulative peak fitting analysis and residual analysis and allows the separation of multiple isobaric peaks not taken into account in the traditional analysis of unit mass resolution squirrel data treatment (Muller et al., 2011). Uncertainties in the major chemical species from the cToF-AMS are typically of the order of ±20% (Drewnick et al., 2005).

213 The PM_1 sea salt concentration was estimated in the cTof-AMS by applying a scaling factor of
214 102 to the ion fragment at 57.98 assigned to NaCl as proposed by (Ovadnevaite et al., 2012).
215 The sea salt-SO_4^{2-} (ss-SO_4^{2-}) was calculated as 0.252 * 0.3 * [seasalt], where 0.252 is the mass
216 ratio of SO_4^{2-} to Na^+ in sea salt and 0.3 is the mass ratio of Na^+ to sea salt (Ghahremaninezhad
217 et al., 2016).

218 Unconstrained positive matrix factorisation was performed on both the unit-mass-resolution
219 spectra of organic aerosol as well as the peak-fitted peaks identified as organics using PMF2
220 v2.08D. This method requires both a matrix for both the organic signals as well as the errors
221 associated with the organics. For the peak-fitted signals, errors for each mass were estimated
222 as

223 $$\frac{\Delta I}{I} = \sqrt{(\alpha^2 t + (\beta + 1)I}$$

224 Where I is the ion signal, ΔI is the absolute uncertainty in the ion signal, α and β are constants
225 (1.2 and 0.001, respectively) and t is the instrumental sampling time in seconds (Drewnick et
226 al., 2009; Allan et al., 2003). For both UMR and peak-fitted inputs, up to 8 factors were
227 investigated by altering the seeds from 0 to 50 in increments of 1 and the fpeaks from -1 to 1
228 in increments of 0.1. Where I is the ion signal, ΔI is the absolute uncertainty in the ion signal,
229 α and β are constants (1.2 and 0.001, respectively) and t is the instrumental sampling time in
230 seconds. For both UMR and peak-fitted inputs, up to 8 factors were investigated by altering
231 the seeds from 0 to 50 in increments of 1 and the fpeaks from -1 to 1 in increments of 0.1.
232 This approach is explained in Ulbrich et al. (2009)

233 2.3.2. Air mass back-trajectory calculation and cluster analysis

234 In order to determine potential source regions for aerosols measured at Lampedusa during
235 the SOP-1a, a series of cluster analyses were performed on HYSPLIT air-mass back-trajectories
236 as per the following. Weekly GDAS1-analysis (Global Data Assimilation System; 1° resolution)
237 trajectory files were downloaded from the Air Resources Laboratory (ARL) of the National
238 Oceanic and Atmospheric Administration (NOAA) archive. 144-hour air-mass backwards
239 trajectories were then calculated every hour over the measurement period with ending point
240 at Lampedusa (height of 45 m) using HYSPLIT (Stein et al., 2015) from within the R-package,
241 SplitR. Cluster analyses were then performed on these calculated trajectories, using a
242 trajectory clustering function within the R-package, OpenAir (Carslaw and Ropkins, 2012).

Clustering was done using two different methods to calculate the similarity between different trajectories. The first uses the Euclidean distance between the latitude and longitude of each trajectory point (a total of 144 in this case, representing each hour prior to the arrival at the receptor site). The second uses the similarity of the angles of each trajectory from the origin. These two methods are described in Sirois and Bottenheim (1995). For each clustering method, the number of clusters was altered from two up to ten. Six clusters identified using the Euclidean-distance method were selected, producing a realistic separation of the air-mass backwards trajectories and distinct and physically meaningful differences in aerosol composition and size. An additional clustering analysis was also performed over 3 and 6 hour intervals and using 96-hour backwards trajectories and yielded similar results.

3. Results and Discussion

3.1. Analysis of local and synoptic meteorology

The analysis of the hourly resolved 144-h air mass backwards trajectories provides an indication of the origin of the air masses sampled at Lampedusa during the field campaign. Six distinct clusters are identified (Figure 2). Cluster 1, "Eastern Mediterranean", is representative of air masses that circulate around the eastern-central Mediterranean basin before arriving at the Lampedusa site (average altitude of 400 m). Cluster 2, "Central Europe" is representative of air masses arriving from central Europe (average altitude of 800 m). Cluster 3, "Atlantic" is representative of more marine-like air masses that predominately originate over the Atlantic Ocean, pass over the Strait of Gibraltar between Spain and Morocco, and cross the western Mediterranean basin (average altitude of 500 m). Cluster 4, "Western Europe", cluster 5, "Mistral (low)", and cluster 6, "Mistral (high)", all have similar angular trajectories, but are distinguishable by their different wind speeds and altitudes (although the Euclidian method of cluster analysis only considers differences in horizontal distances). The two "Mistral" clusters typically originate over the northern Atlantic Ocean, travel over France at a high altitude before descending over the western Mediterranean and travelling with relatively higher wind speeds towards Lampedusa. The altitude of "Mistral (high)" was, on average, higher than "Mistral (low)" (1400 m and 1000 m, respectively) and also coincided with higher wind speeds at Lampedusa (13 ms^{-1} and 9 ms^{-1}, respectively). In comparison, the trajectories of the "Western Europe" cluster spent much more time

circulating at lower altitudes (700 m, on average) over the western Mediterranean basin and, to a certain extent, east of the Lampedusa site.

As a complement, the pressure, temperature, relative humidity, wind speed and direction time series recorded at the station are shown in Figure 3. Two main weather regimes are observed: the former characterized by intense (up to nearly 20 m s^{-1}) northwesterly winds, persisting for several days (10-13 June and 22-30 June) and cool temperatures, whereas the latter associated with low-gradient anticyclonic conditions and light winds from the east or southeast, also favouring warmer temperatures (14-21 June and 1-3 July). Temperatures were relatively stable over the sampling period, fluctuating between approximately 18.5 °C and 28.2 °C. The relative humidity typically ranged from between 70% and 82% with very few and very brief episodes of drier air masses (relative humidity close to or below 50%).

The wind speed and direction distributions during the campaign can be compared to the June-July climatology from 1999 to 2012 (Figure 4). During the sampling period of this study, the frequency of winds from the north-westerly sectors were nearly double the average when compared to normal conditions, approaching 40% with high winds speeds exceeding 10 m s^{-1} observed during more than 20% of the time.

Data of sea level pressure and 1000 mbar meridional wind component composite anomalies obtained from the National Center for Environmental Prediction (NCEP)/National Center for Atmospheric Research (NCAR) Reanalysis (Kalnay et al. 1996) indicate that this particular situation was induced by a “dipolar” pattern, characterized by positive pressure anomalies in the Western Mediterranean and negative ones in the eastern part of the basin (see Supplementary Figure S1). This produced a persisting, stronger than normal gradient over Southern Italy. As a consequence, surface dust episodes typically driven by strong south or southeasterly winds, associated to cyclonic systems moving along northern African coasts, were basically absent during the campaign.

3.2 Aerosol composition

The dry NR-PM_1 concentrations measured at Lampedusa by the cTof-AMS ranged from 1.9 to 33.4 µg m^{-3}, with a mean of 10.2 µg m^{-3} over the sampling period. Sulphate contributed the most to the measured NR-PM_1 mass (41% ± 9% on average) followed by significant contributions from organics (31% ± 8%) and ammonium (17% ± 3%). The eBC, nitrate and sea salt (scaled from the NaCl component of m/z 58) contributed 6% (±4%), 1% (±0.4%) and 3%

(±2%), respectively. Figure 5 shows the total PM_1 concentration (calculated as the sum of the individually measured species), with contribution from each of the species, as well as the calculated PM_1 mass concentration from the SMPS (assuming an average density based on the composition data). There was reasonable agreement between the PM_1 mass concentration calculated from composition measurements and the SMPS, with discrepancy observed during periods of high sulphate concentrations from the eastern Mediterranean, likely due to the broad accumulation mode exceeding the upper size limits of the cToF-AMS inlet. This figure also contains an indication of the air mass origin over the sampling period.

For most of the campaign there was a good agreement between the PM_1 SO_4^{2+} and the TSP SO_4^{2+} concentration, with the exception of periods of high sea salt concentrations when the TSP SO_4^{2+} were significantly higher (see Supplementary Figure S2. Supporting measurements of the size-segregated composition from the cascade impactor corroborate this, indicating a higher contribution of elemental sulphur in the coarse mode during periods of higher sea salt (Supplementary Figure S3). These periods corresponded with the "Mistral" air masses, characterised by higher wind speeds and indicate the role of coarse mode particles in acting as a condensation sink for sulphate species. This indicates that, in these circumstances, the sea salt particles acted as a condensation sink for sulphate precursors. This has important implications for the radiative properties of these aerosols by altering the scattering properties and, potentially cloud condensation nuclei concentrations and composition.

Figure 6 shows the organic mass, split according to different OA factors from the PMF of the OA peaks. From the unconstrained PMF of the UMR and peak-fitted organic mass spectra, the most meaningful solution was found from a 4-factor solution of the UMR analysis (see Supplementary Figures S4 and S5 for the mass reconstruction and time series' residuals). This has resulted in one factor resembling to a primary organic aerosol and three oxygenated organic aerosol (OOA) factors. Herein we label these factors HOA (hydrocarbon-like OA), MO-OOA (more oxidised OOA), LO-OOA (less oxidised OOA) and MSA-OOA (methanesulfonic acid-related OOA).

These factors were compared with ambient organic mass spectra listed in the AMS Spectral Database (Ulbrich et al., 2009). The spectra for the OOA factors (see Figure 7) were strongly correlated with each other ($R > 0.97$) and all three were similar to a "continental" OOA factor observed in a ship campaign in the Artic (Chang et al., 2011), as well as a low-volatility OOA

factor identified in Paris (Crippa et al., 2013). Despite the similarities in their mass spectra, they exhibited different diurnal trends (Figure 7) and time series that were associated with different wind directions and air masses and were therefore not recombined into a single OOA factor.

The MO-OOA factor was the most dominant factor during the field campaign (~53% of the total OA mass) and was typical of low-volatile/highly oxidized OOA observed in many other studies, in the Mediterranean, with high contributions of m/z 44 (f_{44} = 0.31) (e.g. (Hildebrandt et al., 2010; Hildebrandt et al., 2011). This factor was the most prominent during air masses from the Eastern Mediterranean, central Europe and Atlantic (contributing to 71%, 58% and 55% to OA, respectively) and was strongly correlated with ammonium sulphate (R^2 = 0.68) over the whole campaign. It also had a distinct diurnal trend, with concentrations increasing during daylight hours, indicative of photochemical processing. The LO-OOA factor was slightly less oxygenated (f_{44} = 0.26) and exhibited a different time series, related to different air masses, than the MO-OOA. The less oxygenated OOA factor has also been associated with semi-volatile species and is often labelled as SV-OOA (Jimenez et al., 2009). Despite a distinct diurnal profile similar to previously reported SV-OOA factors (with a peak in the early morning), we refrain from labelling our LO-OOA this way because the mass spectrum was generally much more oxygenated and contained less f_{43} than typically reported SV-OOA (see Figure 8).

The MSA-OOA factor contributed approximately 12% of the total OA during the campaign and is likely related to the biogenic emission and processing of dimethyl sulfide (DMS) from phytoplankton in the Mediterranean. This factor was also highly oxygenated (f_{44} = 0.20), but contains key peaks related to the fragmentation of MSA from the electron impact of the cToF-AMS. The most prominent of these peaks were m/z 96 ($CH_4SO_3^+$),79 ($CH_3SO_2^+$), 78 ($CH_2SO_2^+$), 65 (HSO_2^+) and 45 (CHS^+). A similar factor was observed at Bird Island in the south Atlantic Ocean (Schmale et al., 2015), albeit without the contribution of significant m/z 44, suggesting a more aged or mixed aerosol during this campaign. A distinct diurnal pattern for the MSA-OOA was not observed.

While the MO-OOA, LO-OOA and MSA-OOA factors represent secondary organic aerosol and were the most dominant contribution of OA during the campaign (92% on average), a primary organic aerosol factor was observed and identified here as hydrocarbon-like OA (HOA). The mass spectrum of the HOA factor was characteristic of spectra observed in other studies, with

prominent peaks at m/z 95, 91, 83, 81, 71, 69, 57, 55, 43 and 41. Although HOA is typically associated with emissions from incomplete combustion (Zhang et al., 2005), it was not well correlated with other expected tracers such as eBC, CO and NOx. This HOA was typically associated with south-westerly winds of low speed (<5 m s^{-1}; see Figure 9) and peaked at approximately 6 am local time each morning. The poor correlation between the HOA factor and eBC could have been due to a variety of local sources with different HOA and eBC emission factors, a mixing of the PMF factor with some small peaks not associated with combustion processes or from regional HOA that has undergone some transport without significant oxidation. The signal fraction of each m/z of the mass spectrum of the HOA factor however had strong correlations ($0.69 < R < 0.89$) with numerous hydrocarbon-like organic aerosol (HOA) factors from other studies (Hersey et al., 2011; Ulbrich et al., 2009; Ng et al., 2011; Lanz et al., 2007; Zhang et al., 2005) .

3.3 Comparison with other observations around the Mediterranean

There are many factors that could influence the composition, the concentration, and oxidation level of different aerosol species over the Mediterranean. These include different aerosol sources which can follow different seasonal or yearly trends (e.g. biogenic emissions) as well as the existing aerosol load and the meteorological conditions that drive transport, dilution and aging processes. Table 1 summarises the recent observations of NR-PM_1 composition from measurements in the remote Mediterranean.

The majority of previous studies of detailed PM_1 aerosol composition have been taken at coastal sites around the Mediterranean (Mohr et al., 2012; Minguillón et al., 2016; Minguillón et al., 2015; Haddad et al., 2013; Bozzetti et al., 2017) which could be expected to observe higher concentrations than at Lampedusa due to proximity to sources (e.g. traffic, fossil fuel use, heating, biomass burning, industrial activities). Aside from Lampedusa and the observations presented in this study, measurements at Finokalia and Cape Corsica could be considered the most remote sites where these measurements have been taken.

The PM_1 mass loading observed at Lampedusa is comparable to most of these other studies performed at both remote marine sites and coastal sites (see Supplementary Table S1 for a comparison with coastal urban sites). With the exception of Eastern Mediterranean, OA was the dominant NR-PM_1 constituent and summertime OA was generally considered mostly

398 secondary, comprised of SV-OOA and LV-OOA with small contributions of HOA. For remote
399 sites, the results are consistent with a predominance of OA in PM_1 fraction in summer. PMF
400 analysis of Q-AMS measurements at the Finokalia remote site in the eastern Mediterranean
401 in the summer of 2008 showed two OOA factors and a distinct lack of HOA (Hildebrandt et
402 al., 2010). A more recent study during the late 2012 summer at Finokalia observed periods
403 influenced by biomass burning, but otherwise also observed mostly oxygenated organic
404 aerosol (Bougiatioti et al., 2014). Measurements undertaken in the western Mediterranean
405 at Cape Corse from 11 June until 6 August 2013, encompassed the sampling period of this
406 study. For the period from 15 July until 5 August, PMF analysis showed 55%, 27% and 13%
407 contributions of organic matter, sulphate and ammonium to non-refractory PM_1 (Michoud et
408 al., 2017). Secondary oxygenated VOCs dominated the VOC spectrum during the campaign
409 and were very well correlated with submicron organic aerosol. PMF analysis on the OA
410 revealed a 3-factor solution where SV-OOA and LV-OOA were dominant, contributing by 44%
411 and 53%, respectively, with a 4% HOA contribution. From the same measurements but
412 reported over the extended period from 11 June 11 until 5 August 5, there was a higher LV-
413 OOA contribution (62%)(Arndt et al., 2017) which is in agreement with our observations of
414 MO-OOA at Lampedusa. The OA was mostly portioned into MO-OOA and LO-OOA (81%),
415 indicative of well-aged or oxidised secondary organic aerosol from long-range transport of
416 pollutants. Furthermore, the contribution of ammonium sulphate was higher in this study
417 than of all those undertaken in the eastern Mediterranean basin, highlighting the role
418 contribution of sulphates across the Mediterranean.

419 Figure 8 displays the behavior of the f_{44} and f_{43} fragments obtained during the field campaign.
420 f_{44},a proxy for OA oxidation (Jimenez et al., 2009), is calculated as the ratio of the mass at m/z
421 44 (mostly CO_2^+) to the total OA, while f_{43}, equal to the ratio of m/z 43 (mostly $C_2H_3O^+$) to the
422 total OA, typically represents less aged OA. f_{44} was ~0.26 for the majority of the sampling
423 period (Q1; 0.25, Q3: 0.27), while f_{43} was 0.036 (Q1: 0.028, Q3: 0.041). The campaign values
424 are compared to values from the spectra for the four PMF factors and those observed in other
425 field campaigns in the remote Mediterranean. The dotted lines (the so-called "Ng triangle"),
426 encapsulate the f_{44} and f_{43} values of atmospheric OA from a vast number of studies (Ng et al.,
427 2010), with the most aged OA in the top left corner and the most fresh in the bottom right.

The high f_{44} values and the dominance of the highly oxygenated MO-OOA and LO-OOA factors show that the organic aerosol was extremely aged compared to other measurements.

3.4 Links to meteorology

The contribution of the major submicron chemical species and OA sources is further explained in the following by linking the measured and apportioned concentrations to the local meteorology (i.e., wind speed and wind direction) and to the air mass back trajectories to account for the long-range transport of aerosol as well as more distant sources. The bivariate polar plots of these PM_1 species and f_{44} as a function of wind speed and direction are shown in Figure 9.

Considering that the sampling site on Lampedusa is on the north east tip of the island, it is evident that the SO_4^{2-} and NH_4^+ were likely a result of north-westerly marine air masses, in agreement with previous results (e.g., Bove et al., 2016). Sea salt concentrations were highest during high north-westerly wind speeds. Higher concentrations of NO_3^-, HOA and some of the periods with elevated eBC concentrations were observed during low speed south-westerly winds, likely a result of the human settlements and activity on the island of Lampedusa (population of ~6000 located to the south west of the sampling site). Besides, the polar plot for eBC showed a patchier pattern, indicative of more local or point sources and the elevated signals were likely due to air masses passing over ship plumes. Although the mass spectra for the LO-OOA and MO-OOA factors were very similar, their bivariate polar plots indicate different sources or photochemical processes. The MO-OOA was more prominent during north-easterly winds, indicating the most aged organics were influenced by air masses from the eastern Mediterranean, either from long-ranged transport of from circulation of closer pollution sources, while the LO-OOA was more dominant during northwesterly wind directions and air masses from over the western Mediterranean. Figure 10 shows the average contribution of each species during different air mass periods (see Supplementary Table S2 for the mean concentrations and standard deviations).

The highest concentrations of PM_1 were observed during "Eastern Mediterranean" and "Central Europe" air mass periods, when significant lifetime over the lower altitude marine environment and/or higher SO_2 emissions allowed the conversion and condensation of sulphate. These aged aerosols are corroborated by the high number concentrations within the accumulation mode during these periods relative to other periods, measured by the SMPS

as well as the size-resolved sulphate composition, as discussed in the next section. In contrast to the "Eastern Mediterranean" and "Central Europe" air masses, sulphate concentrations were relatively low during the two "Mistral" air masses. This behavior has been found also in PM_{10}, with elevated values of sea salt aerosol and low non-sea salt sulphate during Mistral events (Becagli et al., 2017). The organic mass concentration was relatively uniform across the periods of different air mass origins, with the exception of the high Mistral winds which yielded OA concentrations approximately half the rest of the campaign and a higher contribution of MSA-OOA in comparison with other periods.

3.5 Aerosol size distributions

There are distinctions between the measured PM_1 size distributions during periods of different air mass origins (Figure 11). It should be noted that these size distributions are under ambient conditions without an inlet drier. The ambient relative humidity for each air mass back trajectory cluster was: Eastern Mediterranean (53%), Central Europe (61%), Atlantic (74%), Western Mediterranean (70%), Mistral (low) (67%) and Mistral (high) (74%).

Consistent with the higher concentrations of sulphate and ammonium species, the "Eastern Mediterranean" and "Central Europe" had the most pronounced accumulation modes with respect to those from other clusters due to the presence of accumulation mode sulphate (see Supplementary Figure S6 for the size-resolved chemical composition). In contrast, the "Mistral (high)" air masses had very few particles in the accumulation mode and were mostly dominated by nucleation and Aitken mode particles, in terms of number. There was only one period of "Mistral (high)" air masses, spanning 38 hours between 09:00 on 24 June until 23:00 on 25 June.

The most pronounced new particle formation (NPF) events and subsequent growth were observed during the two "Mistral" air masses, particularly between 25 and 27 June. Very high number concentrations in the nucleation mode were also observed in very brief periods during the Atlantic and, to an extent, the "Western Europe" air masses. There was a no trend (R^2 = 0.03) over the whole campaign between the "nucleation-mode ratio" (defined here as the ratio of particles between 14 and 25 nm and 14 and 600 nm) and the fraction of $CH_3SO_2^+$ (a fragment of MSA, measured by the cToF-AMS) to total PM_1 organics (see Supplementary Figure S7. There was a weak positive trend during periods of the Mistral (high) air mass (R^2 = 0.39). No trends were observed between the nucleation-mode ratio and the occurrence of

other cToF-AMS fragments such as amines that could be linked with biogenic gas-to-particle conversion. Furthermore, there was a weak negative trend between the nucleation-mode ratio and the calculated f_{44} ($R^2 = 0.12$). Without instrumentation to measure the concentration of clusters and smaller aerosols (<14 nm) in conjunction with organic vapours over a longer time period, it is difficult to isolate and conclude the origin of these nucleation particles in a general sense and we will limit our analysis to the most pronounced event during the campaign. Figure 12 shows the size distribution over this period as well as SO_2, eBC and $CH_3SO_2^+$, as well as the back trajectory ending at 04:00 UTC on 25 June at Lampedusa.

This NPF event occurred during the night and therefore in the absence of photochemistry. There was no discernible increase in eBC or SO_2 during these events and the 3-day cascade impactor sample from 25 until 28 June was characterized by the lowest concentrations of vanadium and nickel (released from heavy oil combustion events due to ship emissions) of the whole campaign. The air mass backwards trajectory during this event was characteristic of the "Mistral (high)" cluster. These are high altitude air masses descended over the Atlantic Ocean before having undergone a hydraulic jump over the southern France region and then a rapid descent over the western Mediterranean basin at high speed before arriving at the Lampedusa site. It is interesting to note that these air masses were anomalous for the typical June/July period at Lampedusa. Although the detected mass of $CH_3SO_2^+$ is likely due to the condensation of MSA on accumulation mode particles, and considering that the cTof-AMS collection efficiency below ~100 nm is poor, the increasing concentration of $CH_3SO_2^+$ did coincide with the nucleation events during this period, suggesting a possible nucleation and condensation of marine biogenic vapours. Different studies indicate that NPF events may be triggered by atmospheric mixing processes (Kulmala et al., 2004; Hellmuth, 2006; Lauros et al., 2007; Lauros et al., 2011) due to different phenomena like the enhancement of turbulence in elevated layers (Wehner et al., 2010), the break-up of the nocturnal inversion (Stratmann et al., 2003), or the turbulence associated with the nocturnal low-level jet (Siebert et al., 2007). Furthermore, the intrusion of descending mid-tropospheric air masses in the boundary layer (Pace et al., 2015) has been linked to the occurrence of NPF events and would be consistent with the absence of high concentrations of BC, SO_2, vanadium and nickel which could be expected from ship emissions in the boundary layer over the Mediterranean.

Pace et al. (2006) have shown that clean marine aerosol conditions are rare at Lampedusa and generally associated with north-westerly progressively descending trajectories, in agreement with the findings of this study. The relative absence of pre-existing particles acting as a condensation sink favors NPF events as observed during the field campaign.

3.6 Evidence of aging across the Mediterranean

In order to investigate the aging of aerosols across the north-south trajectory of European continental air masses, we compare the average NR-PM_1 composition measurements at Lampedusa to the concurrent measurements conducted at the Ersa site during summer 2013 (Michoud et al., 2016; Arndt et al., 2017). This is shown in Table 2.

On average, the PM_1 non-refractory organic mass concentrations at both sites were similar with ~3 µg m^{-3}. NO_3^- concentrations were relatively small at both sites, but higher at Ersa (0.28 µg m^{-3}) than at Lampedusa (0.09 µg m^{-3}). Sulphate concentrations were a factor of 3.2 times higher at Lampedusa (4.5 µg m^{-3}) than at Ersa (1.4 µg m^{-3}) while the ammonium concentrations were a factor of 2.7.

To investigate the possible accumulation of ammonium sulphate during the transport of air masses from Europe, the hourly air-mass back trajectories from Lampedusa were filtered so that only those that passed within ±1° latitude and longitude and within ±200 m altitude of the station height of Ersa (550 m) were selected. These thresholds were chosen arbitrarily since there is no clear distinction in horizontal or vertical distance from the site that would necessarily constitute a representative air mass. This resulted in a total of 192 hourly observations at the Ersa site over 32 unique air mass backward trajectory runs (see Figure 13).

These trajectories were grouped mainly into the "Central Europe" cluster (n = 12). The median trajectory duration between the Ersa and Lampedusa sites was 53 hours, with a minimum of 33 hours and a maximum of 144 hours (corresponding to the total duration of the HYSPLIT model runs in this case). Those air masses grouped in the "Eastern Mediterranean" cluster had the longest duration time between the sites of 127 hours (while coincident with the Ersa site, these air masses still spent a significant amount of time over the eastern Mediterranean), followed by "Central Europe" (83 hours), "Western Europe" (45 hours) and then the "Mistral (low)" (38 hours). In general, between the two sites, there was a 40% enhancement in the

organic mass concentration, but an increase in sulphate and ammonium by a factor of 6 and 4, respectively (Table 2).

The accumulation of $(NH_4)_2SO_4$ between Ersa and Lampedusa appeared to be dependent on the travel time of the air mass, however different relationships were observed during different air mass clusters. The total sulphate concentration at Lampedusa minus the total sulphate concentration at Ersa for the same air mass and accounting for the travel time as a function of the travel time is shown in Figure 14.

There was a good positive correlation between the difference in sulphate concentrations between the two sites and the travel time for the "Central Europe" and "Eastern Mediterranean" air masses, while weak positive correlations were observed for the "Western Europe" and "Mistral (low)" clusters. It should be pointed out that the travel time was more than 110 hours for the "Eastern Mediterranean" air masses, while it was only between 33 and 58 hours for the other three air mass clusters. It is expected that the accumulation of sulphate would increase as the total travel time increases due to the opportunity for SO_2 conversion. Although this relationship is somewhat demonstrated here, there are other factors that would influence the SO_4^{2+} accumulation. The sulphate concentrations presented here are measured by an ACSM and cToF-AMS at the Ersa and Lampedusa sites, respectively. Both of these instruments have a 100% inlet efficiency between ~100 nm and 800 nm. The conversion of SO_2 to SO_4^{2-} via nucleation and condensation is dependent on the pre-existing aerosol size distribution and condensation sink. Therefore, the use of PM_1 composition can be misleading if the sulphate is condensing on coarse particles. This is demonstrated in Supplementary Figure S2 that shows the size-resolved mass distribution of sulphur and sodium collected every 3 days on multi-stage cascade impactor filters; the relative contribution of sulphur in the PM_1 is higher than that of PM_{10} in the absence of sodium (a tracer for sea salt). Furthermore, the concentrations of SO_4^{2-} measured by the PILS in the PM_{10} fraction and cToF-AMS in the PM_1 are approximately equal with low sea salt concentrations ($Na+ < 2\ \mu gm^{-3}$), but are nearly a factor of two higher with the PILS for higher sea salt concentrations (Supplementary Figure S3). Furthermore, the emission of SO_2, typically from ships in the Mediterranean, is not necessarily constant over time and is likely not uniformly spread over the basin and within the vertical column (e.g., Becagli et al. (2017)). This could possibly explain the discrepancy between the "growth rate" of sulphate between the Eastern Mediterranean and Central European air mass origins. Furthermore, the sample size for this analysis is

582 relatively small and potentially not representative of the general accumulation of SO_4^{2-} but
583 nonetheless they highlight the magnitude of growth under different air mass trajectories.

4. Concluding remarks

The measurements carried out at Lampedusa during the ChArMEx/ADRIMED SOP-1a field campaign has provided a unique insight into the surface layer aerosols in the remote Central Mediterranean. Air masses were influenced by transport from the eastern Mediterranean, central Europe, the western Europe, the Atlantic Ocean as well as western Europe. Air mass clustering has been performed to explain observed differences in the aerosol composition and size at Lampedusa.

Hourly PM_1 mass ranged from 1.9 to 33.4 μg m^{-3}, with an average of 10.2 μg m^{-3}. It was composed on average of 41% ± 9% sulphate, 31% ± 8% organics, 17% ± 3% ammonium, 6% ± 4% black carbon, 1% ± 0.4% nitrate and 3% ± 2% sea salt. OA was highly oxidized (f_{44} ~0.26), and was apportioned to more oxidised oxygenated OA factor (MO-OOA, 53%), less oxidised OOA factor (LO-OOA, 28%), methanesulfonic acid OOA (MSA-OOA, 12%) and to hydrogen-like OA (HOA, 8%). The highest PM_1 mass loadings were observed for air masses from the Eastern Mediterranean and central Europe, mostly due to the accumulation of ammonium and sulphate. Ancillary data from a remote site at the northern point of Cape Corsica in the Western Mediterranean showed increases of SO_4^{2-} concentrations between 2 and 12 μg m^{-3} when both sites (Corsica and Lampedusa) were connected. Apart from the dominance of ammonium sulphate on the PM_1 composition, the mass concentration and sources of OA have shown to be comparable to previous observations at European coastal and remote sites in the Mediterranean. The most pristine air masses, in terms of PM_1, were observed during periods with north-westerly winds which originated from the western Mediterranean or at high altitudes over the western European continent. Several nucleation and growth events, as well as large sea salt concentrations were observed during these pristine periods. The largest concentrations of PM_1 were observed from air masses from central Europe and those that had circulated over the eastern Mediterranean. In contrast to previous measurements of column-integrated aerosol optical properties (Pace et al., 2006; Meloni et al., 2006), we did not observe the presence of dust or biomass burning in the PM_1 range at the surface.

611 Our results also indicate a clear dichotomy of PM_1 aerosol composition from different source
612 regions. Air masses from central Europe were characterised by a higher organic fraction than
613 those from the eastern Mediterranean, which were enriched in sulphates. This difference
614 could have potential implications on the optical properties and particularly the cloud
615 condensation nuclei capabilities of those air masses. The relative occurrence of easterly air
616 masses is not evident in the climatological wind roses, nor in a previous study by Pace et al.
617 (2006) that took a climatological approach of the air mass back trajectories arriving at
618 Lampedusa from 2001 - 2003. Nonetheless, a re-evaluation of the relative importance and
619 occurrence of different air masses and aerosol properties should be undertaken.
620
621 *Data availability*. Open-access to the data used for this publication is provided to registered
622 users following the data and publication policy of the ChArMEx program
623 (http://mistrals.sedoo.fr/ChArMEx/ Data-Policy/ChArMEx_DataPolicy.pdf). Additional code
624 used in the analysis of data can be obtained upon request from the corresponding or first
625 author. Weekly GDAS1-analysis (Global Data Assimilation System; 1° resolution) trajectory
626 files were downloaded from the Air Resources Laboratory (ARL) of the National Oceanic and
627 Atmospheric Administration (NOAA) archive (ftp://arlftp.arlhq.noaa.gov/archives/gdas1/).
628 144-hour air-mass backwards trajectories were calculated using the R-package, SplitR
629 (https://github.com/rich-iannone/SplitR). Cluster analyses were performed on these
630 calculated trajectories, using the R-package, OpenAir (Carslaw and Ropkins, 2012);
631 https://github.com/cran/openair). Spectra used for comparison of PMF OA factors from
632 those observed in other studies can be found at http://cires.colorado.edu/jimenez-
633 group/AMSsd/
634
635 *Author contributions.* PF, BD, KD, JFD, AGdS designed the experiment in Lampedusa, JS
636 designed the experiment in Ersa, with contributions of co-workers. BD, AM, MCB, FC, GP, KD,
637 CDB, JFD, MM, DM, JS, PZ, AGdS and PF performed the experiments. MDM, BD, AM, GP, KD,
638 JS and PF analysed data and all authors contributed to data interpretation. MDM, BD, GP, KD
639 and PF wrote the manuscript with contributions and/or comments from all co-authors.
640
641 *Competing interests.* The authors declare that they have no conflict of interest.

642

643 *Special issue statement.* This article is part of the special issue of the Chemistry and Aeosols
644 Mediterranean Experiment (ChArMEx) (ACP/AMT inter-journal SI)". It is not associated with
645 a conference.

646

647 *Acknowledgements*. This work is part of the ChArMEx project supported by CNRS-INSU,
648 ADEME, Météo-France and CEA in the framework of the multidisciplinary program MISTRALS
649 (Mediterranean Integrated Studies aT Regional And Local Scales; http://mistrals-home.org/).
650 It has also been supported by the French National Research Agency (ANR) through the
651 ADRIMED program (contract ANR-11-BS56-0006). Measurements at Lampedusa were also
652 supported by the Italian Ministry for University and Research through the NextData and
653 RITMARE Projects. The AERIS national data infrastructure is acknowledged for maintaining
654 the ChArMex database.

655

References

Aiken, A. C., Decarlo, P. F., Kroll, J. H., Worsnop, D. R., Huffman, J. A., Docherty, K. S., Ulbrich, I. M., Mohr, C., Kimmel, J. R., and Sueper, D.: O/C and OM/OC ratios of primary, secondary, and ambient organic aerosols with high-resolution time-of-flight aerosol mass spectrometry, Environmental Science & Technology, 42, 4478-4485, 2008.

Allan, J. D., Jimenez, J. L., Williams, P. I., Alfarra, M. R., Bower, K. N., Jayne, J. T., Coe, H., and Worsnop, D. R.: Quantitative sampling using an Aerodyne aerosol mass spectrometer 1. Techniques of data interpretation and error analysis, Journal of Geophysical Research: Atmospheres, 108, 2003.

Ancellet, G., Pelon, J., Totems, J., Chazette, P., Bazureau, A., Sicard, M., Di Iorio, T., Dulac, F., and Mallet, M.: Long-range transport and mixing of aerosol sources during the 2013 North American biomass burning episode: analysis of multiple lidar observations in the western Mediterranean basin, Atmospheric Chemistry and Physics, 16, 4725-4742, 2016.

Arndt, J., Sciare, J., Mallet, M., Roberts, G. C., Marchand, N., Sartelet, K., Sellegri, K., Dulac, F., Healy, R. M., and Wenger, J. C.: Sources and mixing state of summertime background aerosol in the north-western Mediterranean basin, Atmospheric Chemistry and Physics, 17, 6975-7001, 2017.

Becagli, S., Anello, F., Bommarito, C., Cassola, F., Calzolai, G., Iorio, T. D., Sarra, A. d., Gómez-Amo, J.-L., Lucarelli, F., and Marconi, M.: Constraining the ship contribution to the aerosol of the central Mediterranean, Atmospheric Chemistry and Physics, 17, 2067-2084, 2017.

Bougiatioti, A., Stavroulas, I., Kostenidou, E., Zarmpas, P., Theodosi, C., Kouvarakis, G., Canonaco, F., Prévôt, A., Nenes, A., and Pandis, S.: Processing of biomass-burning aerosol in the eastern Mediterranean during summertime, Atmospheric Chemistry and Physics, 14, 4793-4807, 2014.

Bove, M., Brotto, P., Calzolai, G., Cassola, F., Cavalli, F., Fermo, P., Hjorth, J., Massabò, D., Nava, S., and Piazzalunga, A.: PM10 source apportionment applying PMF and chemical tracer analysis to ship-borne measurements in the Western Mediterranean, Atmospheric Environment, 125, 140-151, 2016.

Bozzetti, C., El Haddad, I., Salameh, D., Daellenbach, K. R., Fermo, P., Gonzalez, R., Minguillón, M. C., Iinuma, Y., Poulain, L., and Elser, M.: Organic aerosol source apportionment by offline-AMS over a full year in Marseille, Atmospheric Chemistry and Physics, 17, 8247-8268, 2017.

Brocchi, V., Krysztofiak, G., Catoire, V., Guth, J., Marécal, V., Zbinden, R., Amraoui, L., Dulac, F., and Ricaud, P.: Intercontinental transport of biomass burning pollutants over the Mediterranean Basin during the summer 2014 ChArMEx-GLAM airborne campaign, Atmospheric Chemistry and Physics, 18, 6887-6906, 2018.

692 Calzolai, G., Nava, S., Lucarelli, F., Chiari, M., Giannoni, M., Becagli, S., Traversi, R., Marconi,
693 M., Frosini, D., and Severi, M.: Characterization of PM 10 sources in the central
694 Mediterranean, Atmospheric Chemistry and Physics, 15, 13939-13955, 2015.

695 Carslaw, D. C., and Ropkins, K.: Openair—an R package for air quality data analysis,
696 Environmental Modelling & Software, 27, 52-61, 2012.

697 Chang, R.-W., Leck, C., Graus, M., Müller, M., Paatero, J., Burkhart, J. F., Stohl, A., Orr, L.,
698 Hayden, K., and Li, S.-M.: Aerosol composition and sources in the central Arctic Ocean during
699 ASCOS, 2011.

700 Chrit, M., Sartelet, K., Sciare, J., Pey, J., Marchand, N., Couvidat, F., Sellegri, K., and Beekmann,
701 M.: Modelling organic aerosol concentrations and properties during ChArMEx summer
702 campaigns of 2012 and 2013 in the western Mediterranean region, Atmospheric Chemistry
703 and Physics, 17, 12509-12531, 2017.

704 Chrit, M., Sartelet, K., Sciare, J., Pey, J., Nicolas, J. B., Marchand, N., Freney, E., Sellegri, K.,
705 Beekmann, M., and Dulac, F.: Aerosol sources in the western Mediterranean during
706 summertime: A model-based approach, Atmos. Chem. Phys. Discuss., https://doi/.
707 org/10.5194/acp-2017-915, in review, 2018.

708 Crippa, M., DeCarlo, P., Slowik, J., Mohr, C., Heringa, M., Chirico, R., Poulain, L., Freutel, F.,
709 Sciare, J., and Cozic, J.: Wintertime aerosol chemical composition and source apportionment
710 of the organic fraction in the metropolitan area of Paris, Atmospheric Chemistry and Physics,
711 13, 961-981, 2013.

712 Crippa, M., Canonaco, F., Lanz, V., Äijälä, M., Allan, J., Carbone, S., Capes, G., Ceburnis, D.,
713 Dall'Osto, M., and Day, D.: Organic aerosol components derived from 25 AMS data sets across
714 Europe using a consistent ME-2 based source apportionment approach, Atmospheric
715 chemistry and physics, 14, 6159-6176, 2014.

716 Denjean, C., Cassola, F., Mazzino, A., Triquet, S., Chevaillier, S., Grand, N., Bourrianne, T.,
717 Momboisse, G., Sellegri, K., and Schwarzenbock, A.: Size distribution and optical properties of
718 mineral dust aerosols transported in the western Mediterranean, Atmospheric Chemistry and
719 Physics, 16, 1081-1104, 2016.

720 Drewnick, F., Hings, S. S., DeCarlo, P., Jayne, J. T., Gonin, M., Fuhrer, K., Weimer, S., Jimenez,
721 J. L., Demerjian, K. L., and Borrmann, S.: A new time-of-flight aerosol mass spectrometer (TOF-
722 AMS)—Instrument description and first field deployment, Aerosol Science and Technology,
723 39, 637-658, 2005.

724 Drewnick, F., Hings, S., Alfarra, M., Prevot, A., and Borrmann, S.: Aerosol quantification with
725 the Aerodyne Aerosol Mass Spectrometer: detection limits and ionizer background effects,
726 Atmos. Meas. Tech., 2, 33-46, 2009.

727 Formenti, P., Boucher, O., Reiner, T., Sprung, D., Andreae, M. O., Wendisch, M., Wex, H.,
728 Kindred, D., Tzortziou, M., and Vasaras, A.: STAAARTE-MED 1998 summer airborne
729 measurements over the Aegean Sea 2. Aerosol scattering and absorption, and radiative
730 calculations, Journal of Geophysical Research: Atmospheres, 107, 2002.

731 Formenti, P., Mbemba Kabuiku, L., Chiapello, I., Ducos, F., Dulac, F., and Tanré, D.: Aerosol
732 optical properties derived from POLDER-3/PARASOL (2005–2013) over the western
733 Mediterranean Sea: I. Quality assessment with AERONET and in situ airborne observations,
734 Atmos. Meas. Tech. Discuss., https://doi.org/10.5194/amt-2018-251, 2018.

735 Ghahremaninezhad, R., Norman, A.-L., Abbatt, J. P., Levasseur, M., and Thomas, J. L.: Biogenic,
736 anthropogenic and sea salt sulfate size-segregated aerosols in the Arctic summer,
737 Atmospheric Chemistry and Physics, 16, 5191-5202, 2016.

738 Haddad, I. E., D'Anna, B., Temime-Roussel, B., Nicolas, M., Boreave, A., Favez, O., Voisin, D.,
739 Sciare, J., George, C., and Jaffrezo, J.-L.: Towards a better understanding of the origins,
740 chemical composition and aging of oxygenated organic aerosols: case study of a
741 Mediterranean industrialized environment, Marseille, Atmospheric Chemistry and Physics,
742 13, 7875-7894, 2013.

743 Haywood, J., and Boucher, O.: Estimates of the direct and indirect radiative forcing due to
744 tropospheric aerosols: A review, Reviews of geophysics, 38, 513-543, 2000.

745 Hellmuth, O.: Columnar modelling of nucleation burst evolution in the convective boundary
746 layer–first results from a feasibility study Part IV: A compilation of previous observations for
747 valuation of simulation results from a columnar modelling study, Atmospheric Chemistry and
748 Physics, 6, 4253-4274, 2006.

749 Hersey, S., Craven, J., Schilling, K., Metcalf, A., Sorooshian, A., Chan, M., Flagan, R., and
750 Seinfeld, J.: The Pasadena Aerosol Characterization Observatory (PACO): chemical and
751 physical analysis of the Western Los Angeles basin aerosol, Atmospheric Chemistry and
752 Physics, 11, 7417-7443, 2011.

753 Hildebrandt, L., Engelhart, G., Mohr, C., Kostenidou, E., Lanz, V., Bougiatioti, A., DeCarlo, P.,
754 Prevot, A., Baltensperger, U., and Mihalopoulos, N.: Aged organic aerosol in the Eastern
755 Mediterranean: the Finokalia Aerosol Measurement Experiment–2008, Atmospheric
756 Chemistry and Physics, 10, 4167-4186, 2010.

757 Hildebrandt, L., Kostenidou, E., Lanz, V., Prevot, A., Baltensperger, U., Mihalopoulos, N.,
758 Laaksonen, A., Donahue, N. M., and Pandis, S. N.: Sources and atmospheric processing of
759 organic aerosol in the Mediterranean: insights from aerosol mass spectrometer factor
760 analysis, Atmospheric Chemistry and Physics, 11, 12499-12515, 2011.

761 Jimenez, J. L., Canagaratna, M., Donahue, N., Prevot, A., Zhang, Q., Kroll, J. H., DeCarlo, P. F.,
762 Allan, J. D., Coe, H., and Ng, N.: Evolution of organic aerosols in the atmosphere, science, 326,
763 1525-1529, 2009.

764 Koçak, M., Mihalopoulos, N., and Kubilay, N.: Chemical composition of the fine and coarse
765 fraction of aerosols in the northeastern Mediterranean, Atmospheric Environment, 41, 7351-
766 7368, 2007.

767 Koulouri, E., Saarikoski, S., Theodosi, C., Markaki, Z., Gerasopoulos, E., Kouvarakis, G., Mäkelä,
768 T., Hillamo, R., and Mihalopoulos, N.: Chemical composition and sources of fine and coarse

769 aerosol particles in the Eastern Mediterranean, Atmospheric Environment, 42, 6542-6550,
770 2008.

771 Kulmala, M., Vehkamäki, H., Petäjä, T., Dal Maso, M., Lauri, A., Kerminen, V.-M., Birmili, W.,
772 and McMurry, P.: Formation and growth rates of ultrafine atmospheric particles: a review of
773 observations, Journal of Aerosol Science, 35, 143-176, 2004.

774 Lanz, V. A., Alfarra, M. R., Baltensperger, U., Buchmann, B., Hueglin, C., Szidat, S., Wehrli, M.
775 N., Wacker, L., Weimer, S., and Caseiro, A.: Source attribution of submicron organic aerosols
776 during wintertime inversions by advanced factor analysis of aerosol mass spectra,
777 Environmental science & technology, 42, 214-220, 2007.

778 Lauros, J., Nilsson, E., Maso, M. D., and Kulmala, M.: Contribution of mixing in the ABL to new
779 particle formation based on observations, Atmospheric Chemistry and Physics, 7, 4781-4792,
780 2007.

781 Lauros, J., Sogachev, A., Smolander, S., Vuollekoski, H., Sihto, S.-L., Mammarella, I., Laakso, L.,
782 Rannik, Ü., and Boy, M.: Particle concentration and flux dynamics in the atmospheric
783 boundary layer as the indicator of formation mechanism, Atmospheric Chemistry and Physics,
784 11, 5591-5601, 2011.

785 Lelieveld, J., Berresheim, H., Borrmann, S., Crutzen, P., Dentener, F., Fischer, H., Feichter, J.,
786 Flatau, P., Heland, J., and Holzinger, R.: Global air pollution crossroads over the
787 Mediterranean, Science, 298, 794-799, 2002.

788 Mallet, M., Dulac, F., Formenti, P., Nabat, P., Sciare, J., Roberts, G., Pelon, J., Ancellet, G.,
789 Tanré, D., and Parol, F.: Overview of the chemistry-aerosol Mediterranean
790 experiment/aerosol direct radiative forcing on the Mediterranean climate
791 (ChArMEx/ADRIMED) summer 2013 campaign, Atmospheric Chemistry and Physics, 16, 455-
792 504, 2016.

793 Mariotti, A., Pan, Y., Zeng, N., and Alessandri, A.: Long-term climate change in the
794 Mediterranean region in the midst of decadal variability, Climate Dynamics, 44, 1437-1456,
795 2015.

796 Meloni, D., Sarra, A. d., Pace, G., and Monteleone, F.: Aerosol optical properties at Lampedusa
797 (Central Mediterranean). 2. Determination of single scattering albedo at two wavelengths for
798 different aerosol types, Atmospheric Chemistry and Physics, 6, 715-727, 2006.

799 Michoud, V., Sciare, J., Sauvage, S., Dusanter, S., Léonardis, T., Gros, V., Kalogridis, C., Zannoni,
800 N., Féron, A., and Petit, J.-E.: Organic carbon at a remote site of the western Mediterranean
801 Basin: sources and chemistry during the ChArMEx SOP2 field experiment, Atmospheric
802 chemistry and physics, 17, 8837-8865, 2017.

803 Minguillón, M., Pérez, N., Marchand, N., Bertrand, A., Temime-Roussel, B., Agrios, K., Szidat,
804 S., van Drooge, B., Sylvestre, A., and Alastuey, A.: Secondary organic aerosol origin in an urban
805 environment: influence of biogenic and fuel combustion precursors, Faraday Discuss, 189,
806 337-359, 2016.

807 Minguillón, M. C., Ripoll, A., Pérez, N., Prévôt, A., Canonaco, F., Querol, X., and Alastuey, A.:
808 Chemical characterization of submicron regional background aerosols in the western
809 Mediterranean using an Aerosol Chemical Speciation Monitor, Atmospheric Chemistry and
810 Physics, 15, 6379-6391, 2015.

811 Mohr, C., DeCarlo, P., Heringa, M., Chirico, R., Slowik, J., Richter, R., Reche, C., Alastuey, A.,
812 Querol, X., and Seco, R.: Identification and quantification of organic aerosol from cooking and
813 other sources in Barcelona using aerosol mass spectrometer data, Atmospheric Chemistry
814 and Physics, 12, 1649-1665, 2012.

815 Muller, M., George, C., and D'Anna, B.: Enhanced spectral analysis of C-TOF Aerosol Mass
816 Spectrometer data: iterative residual analysis and cumulative peak fitting, INTERNATIONAL
817 JOURNAL OF MASS SPECTROMETRY, 306, 1-8, 2011.

818 Ng, N., Canagaratna, M., Zhang, Q., Jimenez, J., Tian, J., Ulbrich, I., Kroll, J., Docherty, K.,
819 Chhabra, P., and Bahreini, R.: Organic aerosol components observed in Northern Hemispheric
820 datasets from Aerosol Mass Spectrometry, Atmospheric Chemistry and Physics, 10, 4625-
821 4641, 2010.

822 Ng, N., Canagaratna, M., Jimenez, J., Chhabra, P., Seinfeld, J., and Worsnop, D.: Changes in
823 organic aerosol composition with aging inferred from aerosol mass spectra, Atmospheric
824 Chemistry and Physics, 11, 6465-6474, 2011.

825 Orsini, D. A., Ma, Y., Sullivan, A., Sierau, B., Baumann, K., and Weber, R. J.: Refinements to the
826 particle-into-liquid sampler (PILS) for ground and airborne measurements of water soluble
827 aerosol composition, Atmospheric Environment, 37, 1243-1259, 2003.

828 Ortiz-Amezcua, P., Guerrero-Rascado, J., Granados-Muñoz, M., Bravo-Aranda, J., and Alados-
829 Arboledas, L.: Characterization of atmospheric aerosols for a long range transport of biomass
830 burning particles from canadian forest fires over the southern iberian peninsula in July 2013,
831 Optica Pura y Aplicada, 47, 43-49, 2014.

832 Ovadnevaite, J., Ceburnis, D., Canagaratna, M., Berresheim, H., Bialek, J., Martucci, G.,
833 Worsnop, D. R., and O'Dowd, C.: On the effect of wind speed on submicron sea salt mass
834 concentrations and source fluxes, Journal of Geophysical Research: Atmospheres (1984–
835 2012), 117, 2012.

836 Paatero, P., and Tapper, U.: Positive matrix factorization: A non-negative factor model with
837 optimal utilization of error estimates of data values, Environmetrics, 5, 111-126, 1994.

838 Paatero, P.: Least squares formulation of robust non-negative factor analysis, Chemometrics
839 and intelligent laboratory systems, 37, 23-35, 1997.

840 Pace, G., Meloni, D., and Di Sarra, A.: Forest fire aerosol over the Mediterranean basin during
841 summer 2003, Journal of Geophysical Research: Atmospheres, 110, 2005.

842 Pace, G., Sarra, A. d., Meloni, D., Piacentino, S., and Chamard, P.: Aerosol optical properties
843 at Lampedusa (Central Mediterranean). 1. Influence of transport and identification of
844 different aerosol types, Atmospheric Chemistry and Physics, 6, 697-713, 2006.

Pace, G., Junkermann, W., Vitali, L., Di Sarra, A., Meloni, D., Cacciani, M., Cremona, G., Iannarelli, A. M., and Zanini, G.: On the complexity of the boundary layer structure and aerosol vertical distribution in the coastal Mediterranean regions: a case study, Tellus B: Chemical and Physical Meteorology, 67, 27721, 2015.

Perrone, M., and Bergamo, A.: Direct radiative forcing during Sahara dust intrusions at a site in the Central Mediterranean: Anthropogenic particle contribution, Atmospheric research, 101, 783-798, 2011.

Perrone, M., Becagli, S., Orza, J. G., Vecchi, R., Dinoi, A., Udisti, R., and Cabello, M.: The impact of long-range-transport on PM1 and PM2. 5 at a Central Mediterranean site, Atmospheric environment, 71, 176-186, 2013.

Petit, J.-E., Favez, O., Albinet, A., and Canonaco, F.: A user-friendly tool for comprehensive evaluation of the geographical origins of atmospheric pollution: Wind and trajectory analyses, Environmental Modelling & Software, 88, 183-187, 2017.

Pikridas, M., Riipinen, I., Hildebrandt, L., Kostenidou, E., Manninen, H., Mihalopoulos, N., Kalivitis, N., Burkhart, J. F., Stohl, A., and Kulmala, M.: New particle formation at a remote site in the eastern Mediterranean, Journal of Geophysical Research: Atmospheres, 117, 2012.

Querol, X., Alastuey, A., Pey, J., Cusack, M., Pérez, N., Mihalopoulos, N., Theodosi, C., Gerasopoulos, E., Kubilay, N., and Koçak, M.: Variability in regional background aerosols within the Mediterranean, Atmospheric Chemistry and Physics, 9, 4575-4591, 2009a.

Querol, X., Pey, J., Pandolfi, M., Alastuey, A., Cusack, M., Pérez, N., Moreno, T., Viana, M., Mihalopoulos, N., and Kallos, G.: African dust contributions to mean ambient PM10 mass-levels across the Mediterranean Basin, Atmospheric Environment, 43, 4266-4277, 2009b.

Rinaldi, M., Gilardoni, S., Paglione, M., Sandrini, S., Decesari, S., Zanca, N., Marinoni, A., Cristofanelli, P., Bonasoni, P., and Ielpo, P.: Physico-chemical characterization of Mediterranean background aerosol at the Capogranitola observatory (Sicily), EGU General Assembly Conference Abstracts, 2017, 3161.

Sanchez-Gomez, E., Somot, S., and Mariotti, A.: Future changes in the Mediterranean water budget projected by an ensemble of regional climate models, Geophysical Research Letters, 36, 2009.

Schembari, C., Bove, M., Cuccia, E., Cavalli, F., Hjorth, J., Massabò, D., Nava, S., Udisti, R., and Prati, P.: Source apportionment of PM10 in the Western Mediterranean based on observations from a cruise ship, Atmospheric environment, 98, 510-518, 2014.

Schmale, J., Schneider, J., Nemitz, E., Tang, Y., Dragosits, U., Blackall, T., Trathan, P., Phillips, G., Sutton, M., and Braban, C.: Sub-Antarctic marine aerosol: dominant contributions from biogenic sources, Atmospheric Chemistry and Physics, 13, 8669-8694, 2013.

Sciare, J., Bardouki, H., Moulin, C., and Mihalopoulos, N.: Aerosol sources and their contribution to the chemical composition of aerosols in the Eastern Mediterranean Sea during summertime, Atmospheric Chemistry and Physics, 3, 291-302, 2003.

Sciare, J., Oikonomou, K., Favez, O., Liakakou, E., Markaki, Z., Cachier, H., and Mihalopoulos, N.: Long-term measurements of carbonaceous aerosols in the Eastern Mediterranean: evidence of long-range transport of biomass burning, Atmospheric Chemistry and Physics, 8, 5551-5563, 2008.

Siebert, H., Wehner, B., Hellmuth, O., Stratmann, F., Boy, M., and Kulmala, M.: New-particle formation in connection with a nocturnal low-level jet: Observations and modeling results, Geophysical Research Letters, 34, 2007.

Sirois, A., and Bottenheim, J. W.: Use of backward trajectories to interpret the 5-year record of PAN and O3 ambient air concentrations at Kejimkujik National Park, Nova Scotia, Journal of Geophysical Research: Atmospheres, 100, 2867-2881, 1995.

Stein, A., Draxler, R. R., Rolph, G. D., Stunder, B. J., Cohen, M., and Ngan, F.: NOAA's HYSPLIT atmospheric transport and dispersion modeling system, Bulletin of the American Meteorological Society, 96, 2059-2077, 2015.

Stohl, A., Forster, C., Frank, A., Seibert, P., and Wotawa, G.: The Lagrangian particle dispersion model FLEXPART version 6.2, Atmospheric Chemistry and Physics, 5, 2461-2474, 2005.

Stratmann, F., Siebert, H., Spindler, G., Wehner, B., Althausen, D., Heintzenberg, J., Hellmuth, O., Rinke, R., Schmieder, U., and Seidel, C.: New-particle formation events in a continental boundary layer: first results from the SATURN experiment, Atmospheric Chemistry and Physics, 3, 1445-1459, 2003.

Tadros, C. V., Crawford, J., Treble, P. C., Baker, A., Cohen, D. D., Atanacio, A. J., Hankin, S., and Roach, R.: Chemical characterisation and source identification of atmospheric aerosols in the Snowy Mountains, south-eastern Australia, Science of The Total Environment, 630, 432-443, 2018.

Ulbrich, I., Canagaratna, M., Zhang, Q., Worsnop, D., and Jimenez, J.: Interpretation of organic components from Positive Matrix Factorization of aerosol mass spectrometric data, Atmospheric Chemistry and Physics, 9, 2891-2918, 2009.

Wehner, B., Siebert, H., Ansmann, A., Ditas, F., Seifert, P., Stratmann, F., Wiedensohler, A., Apituley, A., Shaw, R., and Manninen, H.: Observations of turbulence-induced new particle formation in the residual layer, Atmospheric chemistry and physics, 10, 4319-4330, 2010.

World Health Organization.: Ambient air pollution: A global assessment of exposure and burden of disease, 2016.

Zhang, H., Surratt, J., Lin, Y., Bapat, J., and Kamens, R.: Effect of relative humidity on SOA formation from isoprene/NO photooxidation: enhancement of 2-methylglyceric acid and its corresponding oligoesters under dry conditions, Atmospheric Chemistry and Physics, 11, 6411-6424, 2011.

Zhang, Q., Worsnop, D., Canagaratna, M., and Jimenez, J. L.: Hydrocarbon-like and oxygenated organic aerosols in Pittsburgh: insights into sources and processes of organic aerosols, Atmospheric Chemistry and Physics, 5, 3289-3311, 2005.

922 Zhou, S., Collier, S., Xu, J., Mei, F., Wang, J., Lee, Y. N., Sedlacek, A. J., Springston, S. R., Sun,
923 Y., and Zhang, Q.: Influences of upwind emission sources and atmospheric processing on
924 aerosol chemistry and properties at a rural location in the Northeastern US, Journal of
925 Geophysical Research: Atmospheres, 121, 6049-6065, 2016.
926
927

Atmos. Chem. Phys. Discuss., https://doi.org/10.5194/acp-2019-192
Manuscript under review for journal Atmos. Chem. Phys.
Discussion started: 12 March 2019

Atmospheric Chemistry and Physics Discussions

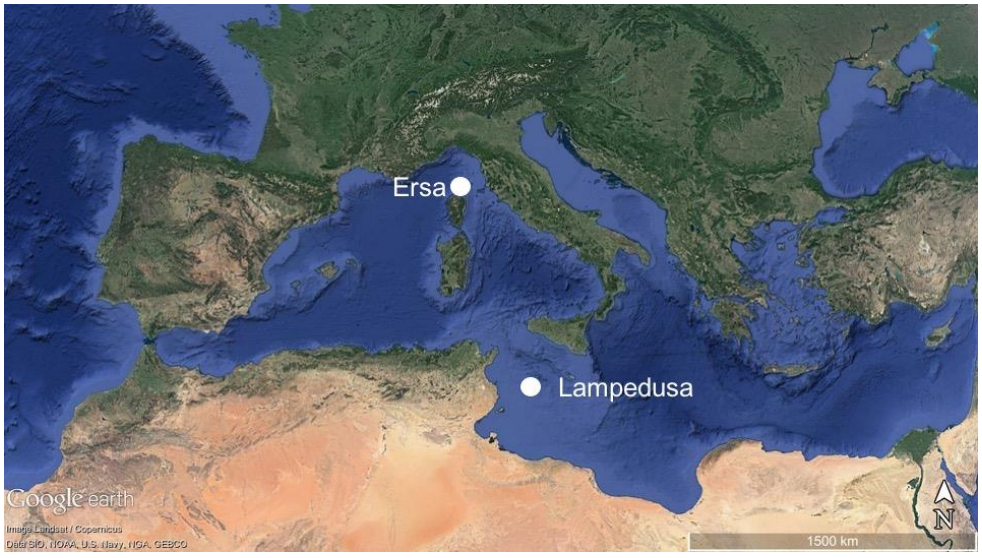

928

929 *Figure 1 The Mediterranean basin. The two sites considered in this study, Lampedusa and Ersa, are indicated with white*
930 *dots. Image is courtesy of Google Earth.*

931

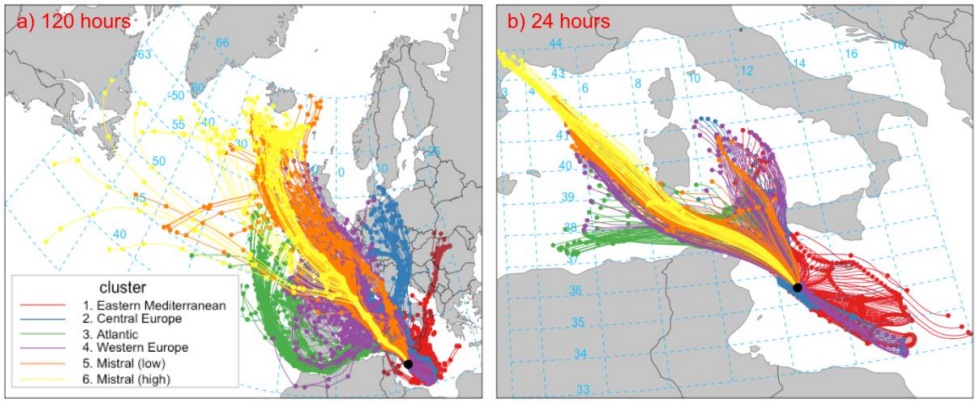

932
933 *Figure 2 a) Hourly 144-hour (6 days) backwards trajectories from Lampedusa from 10 June 2013 until 5 July 2013, cut off at*
934 *120 hours (5 days). Colors represent the assigned cluster. B) The same as a) but cut off at 24-hour.*

Atmos. Chem. Phys. Discuss., https://doi.org/10.5194/acp-2019-192
Manuscript under review for journal Atmos. Chem. Phys.
Discussion started: 12 March 2019

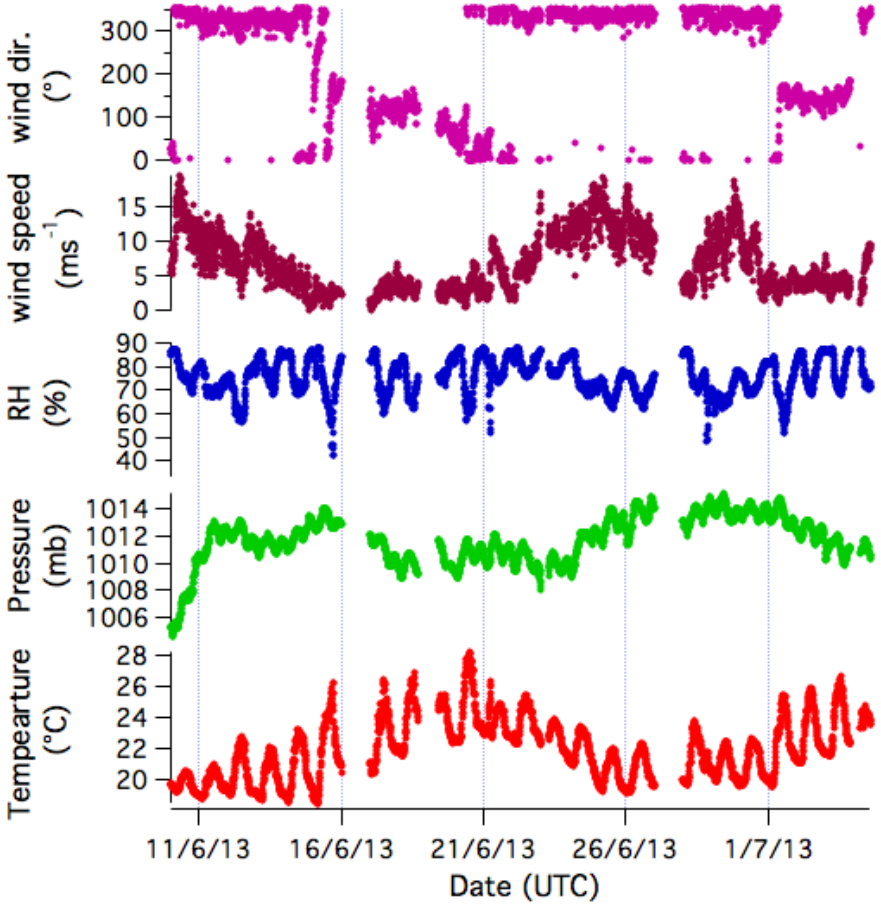

Figure 3 Meteorological conditions (wind direction and speed, relative humidity, pressure and temperature) measured at the Lampedusa site during SOP-1a.

Atmos. Chem. Phys. Discuss., https://doi.org/10.5194/acp-2019-192
Manuscript under review for journal Atmos. Chem. Phys.
Discussion started: 12 March 2019

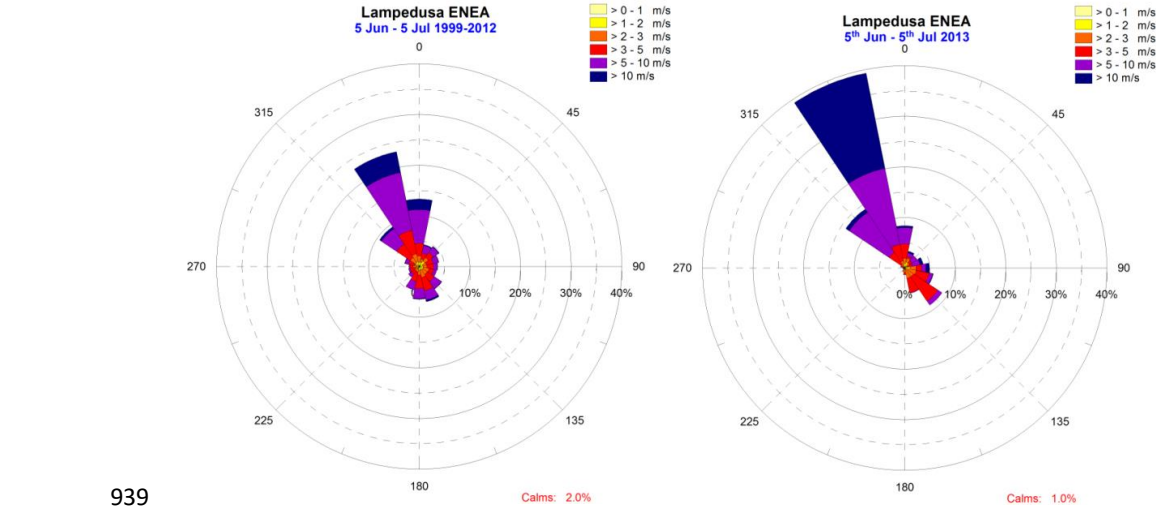

939

940 *Figure 4 Wind speed and direction at Lampedusa during the period from 5 June until 5 July during the years from 1999 - 2012*
941 *(left) and during this campaign (right).*

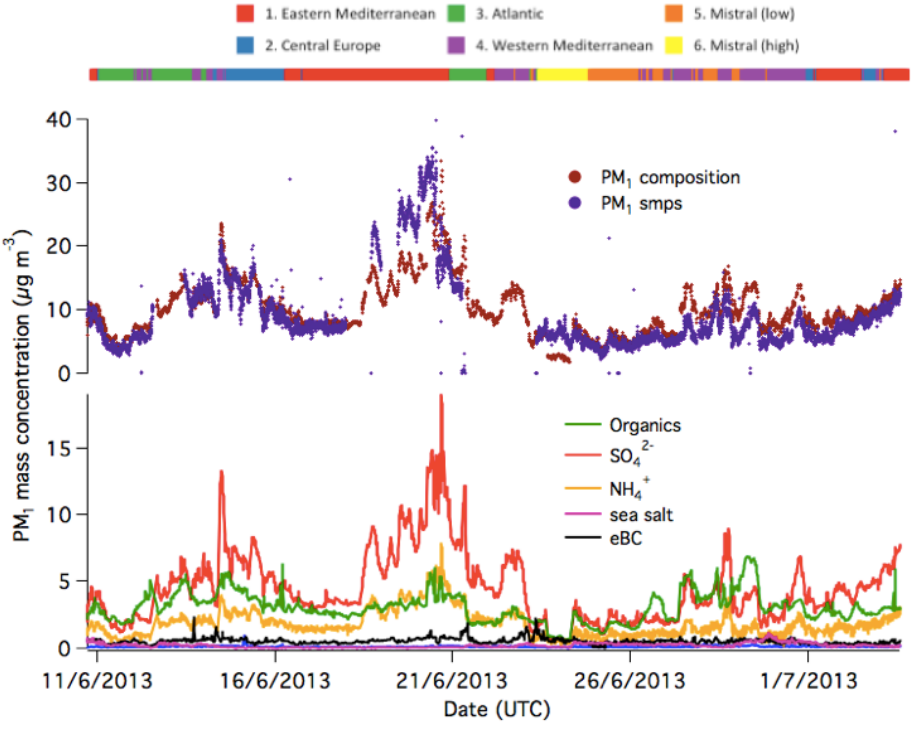

942

943 *Figure 5 The time series of PM_1 mass concentration, coloured by the relative contribution from each species. The top bar is*
944 *coloured according to the air mass origin.*

Atmos. Chem. Phys. Discuss., https://doi.org/10.5194/acp-2019-192
Manuscript under review for journal Atmos. Chem. Phys.
Discussion started: 12 March 2019

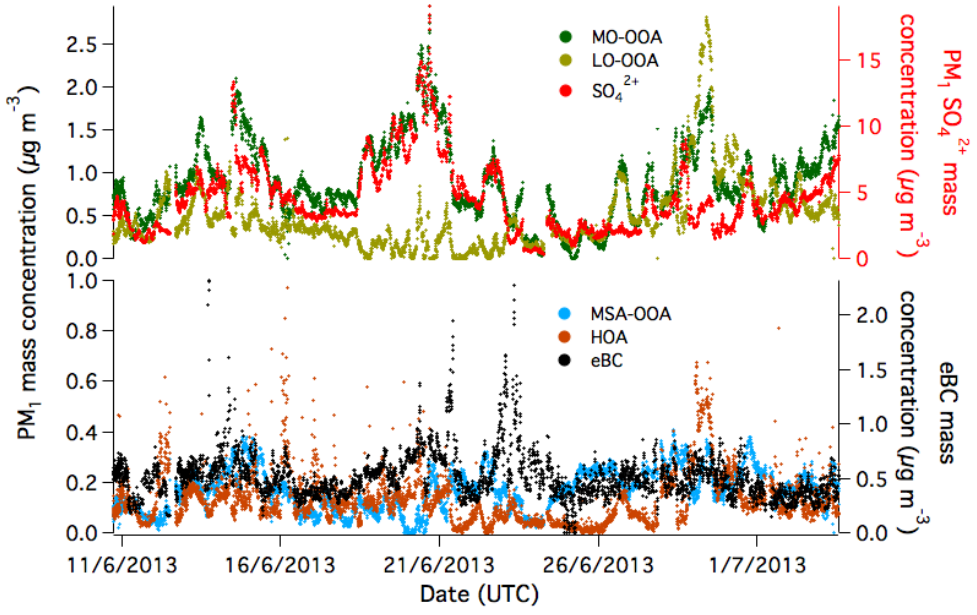

Figure 6 The time series of the PM_1 "more oxidised" OOA (MO-OOA), "less oxidised" (OOA) and sulphate (top panel) and methanesulfonic acid-related OOA (MSA-OOA), hydrocarbon-like OA (HOA) and eBC (bottom panel).

Atmos. Chem. Phys. Discuss., https://doi.org/10.5194/acp-2019-192
Manuscript under review for journal Atmos. Chem. Phys.
Discussion started: 12 March 2019

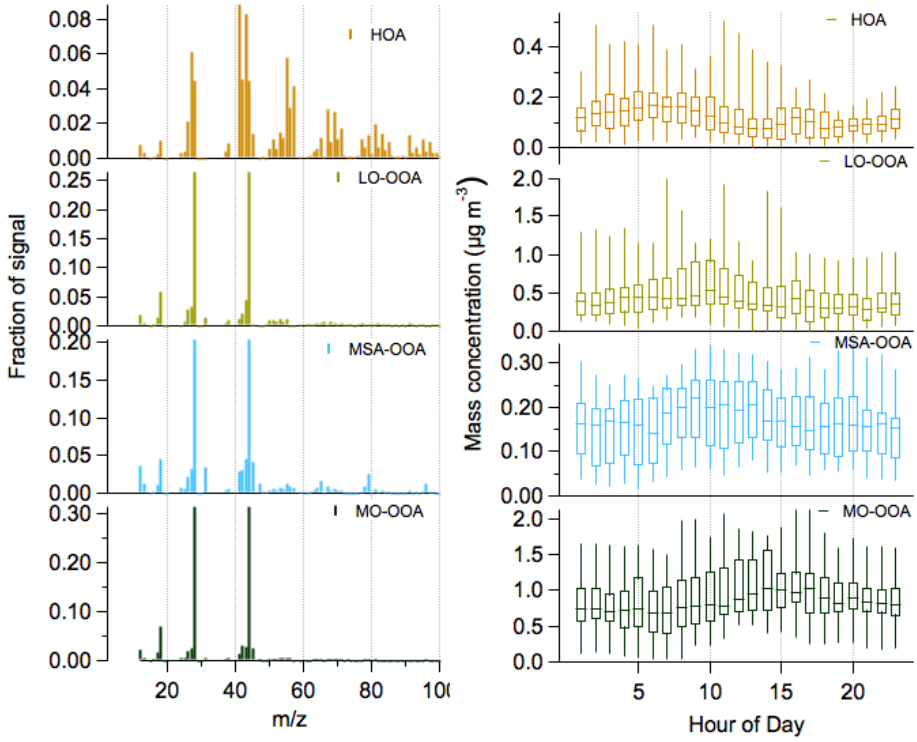

Figure 7 The mass spectra for the 4 PMF factors (HOA: hydrocarbon-like organic aerosol, LO-OOA: less oxidised OOA, MO-OOA: more oxidised OOA, MSA-OOA: methanesulfonic acid-related OOA) retrieved from the PMF analysis of unit-mass resolution data.

Table 1 A summary of studies that have investigated NR-PM$_1$ composition (including PMF of OA) on islands within the Mediterranean basin and at coastal sites surrounding the basin. Only studies that have investigated PMF-based OA source apportionment are reported. HOA: Hydrocarbon-like Organic Aerosol, SV-OOA: Semi-volatile oxygenated Organic Aerosol, LV-OOA: Low-volatility oxygenated Organic Aerosol, BBOA: Biomass burning Organic Aerosol, COA: Cooking Organic Aerosol, OOA: Oxygenated Organic Aerosol, F4: "Factor -4" (unidentified PMF factor), IndOA: Industry-related Organic Aerosol, OB-OA: "Olive-branch Organic Aerosol. PMF factors in bold indicate secondary organic aerosol. After the results of this study, observations are ordered according to longitude (west to east).

AUTHORS (YEAR)	LOCATION	PERIOD	INSTRUMENT	PM$_1$ MASS AND COMPOSITION	PMF FACTORS
THIS STUDY	Lampedusa (35°31'5"N, 12°37'51"E, 45 m a.s.l.)	10 June - 5 July 2013 (summer)	cToF-AMS	10.1 µg m^{-3} (OA: 30%, SO_4^{2-}: 44%, NH_4^+: 18%, NO_3^-: 1%, seasalt: 1%, eBC: 5%)	HOA (8%) **MSA-OOA (12%)** **LO-OOA (28%)** **MO-OOA (53%)**

(MINGUILLÓN ET AL., 2015)	Montseny (41°46'46"N, 02°21'19"E, 720 m a.s.l.)	June 2012 - July 2013	ACSM	Summer: 10.8 µg m^{-3} (OA: 60%, SO_4^{2-}: 20%, NH_4^+: %, NO_3^-: %, Winter: 6.3 µg m^{-3} (OA:, SO_4^{2-}: 8%, NH_4^+: %, NO_3^-: %,	Summer: HOA (13%) **SV-OOA (41%)** **LV-OOA (44%)** Winter: HOA (12%) BBOA (28%) **OOA (59%)**
(ARNDT ET AL., 2017)	Cape Corse (42°58'8.4"N, 9°22'48"E, 544 m a.s.l.)	11 June - 6 August 2013 (Summer)	Q-ACSM	5.5 µg m^{-3} (OA: 55%, SO_4^{2-}: 26, NH_4^+: 13%, NO_3^-: 5%)	**SV-OOA (62%)** **LV-OOA (33%)**
(MICHOUD ET AL., 2017)	Cape Corse (42°58'8.4"N, 9°22'48"E, 544 m a.s.l.)	July 15 - August 5 2013 (Summer)	Q-ACSM	6.8 µg m^{-3} (OA: 55%, SO_4^{2-}: 27%, NH_4^+: 13%, NO_3^-: 5%)	HOA (4%) **SV-OOA (44%)** **LV-OOA(53%)**
(RINALDI ET AL., 2017)	Cape Granitola (37°34'31.1"N, 12°39'34.2"E, 5 m a.s.l.)	April 2016 (Spring)	HR-ToF-AMS	3.5 µg m^{-3} (OA: 37%, SO_4^{2-}: 31%, NH_4^+: 12%, NO_3^-: 3%, seasalt: 10%, BC: 6%)	HOA (3%) BBOA (2%) **OOA-1 + OOA-2 (70%)** **OOA-3 (25%)**
HILDEBREANDT ET AL., 2010	Finokalia (35°20'N, 25°40'E, 150 m a.s.l.)	May 2008 (Spring)	Q-AMS	9 µg m^{-3} (OA: 28%, SO_4^{2-}: 55%, NH_4^+: 16%, NO_3^-: 2%)	OOA-1 (61%) OOA-2 (39%)
HILDEBRAND ET AL., 2011	Finokalia (35°20'N, 25°40'E, 150 m a.s.l.)	25 February - 26 March 2009 (late Winter)	Q-AMS	3.3 µg m^{-3} (OA: 43%, SO_4^{2-}: 42%, NH_4^+: 14%, NO_3^-: 2%)	**OOA (>56%)** OB-OA (15 - 35%) Amine-OA (6 - 21%)
BOUGIATIOTI ET AL., 2014	Finokalia (35°20'N, 25°40'E, 150 m a.s.l.)	August - September 2012	Q-ACSM	Fire events: OA: 46.5% , SO_4^{2-}: 29.2%, NH_4^+: 11.7%, NO_3^-: 3.2%, BC: 9.5% Nonfire periods: OA: 34.7% , SO_4^{2-}: 43%, NH_4^+: 13.7%, NO_3^-: 2.2%, BC: 6.1%	BBOA (<20%) **OOA1-BB + OOA2 (>80%)**

Atmos. Chem. Phys. Discuss., https://doi.org/10.5194/acp-2019-192
Manuscript under review for journal Atmos. Chem. Phys.
Discussion started: 12 March 2019

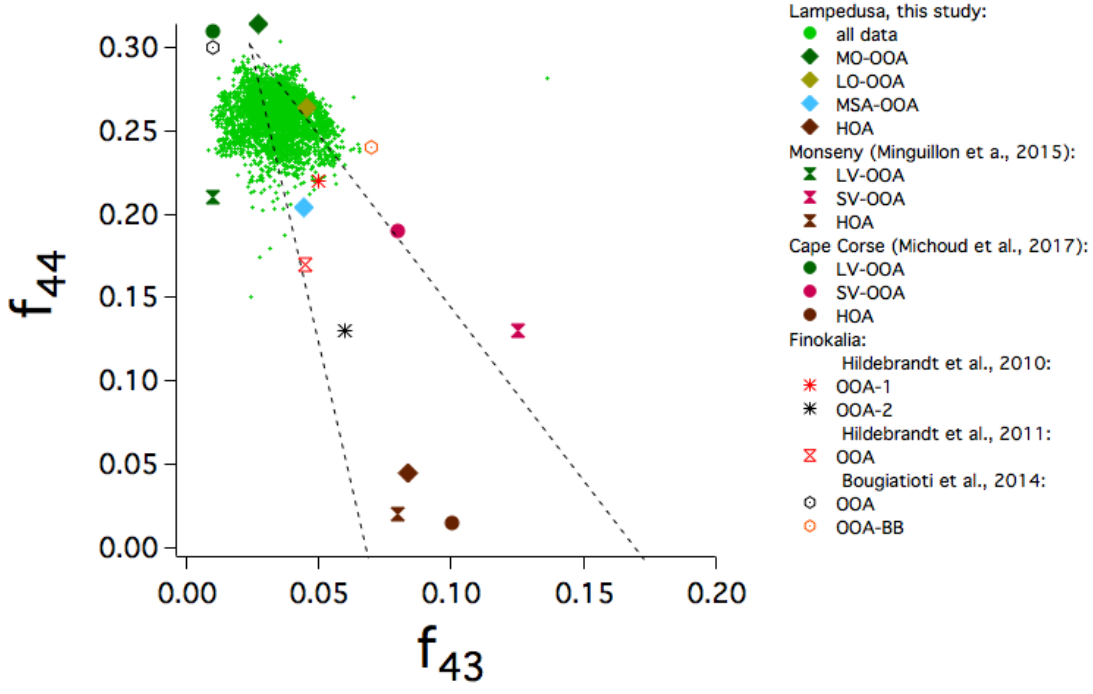

961

962 *Figure 8 f_{43} (the ratio of m/z 43 to the total OA)* against f_{44} (ratio of m/z 44 to the total OA). The triangle is considered to
963 encapsulate typical atmospheric values of OA according to Ng et al. (2010). The values for the various PMF factors from this
964 study and other studies conducted in the remote Mediterranean are also displayed.

Atmos. Chem. Phys. Discuss., https://doi.org/10.5194/acp-2019-192
Manuscript under review for journal Atmos. Chem. Phys.
Discussion started: 12 March 2019

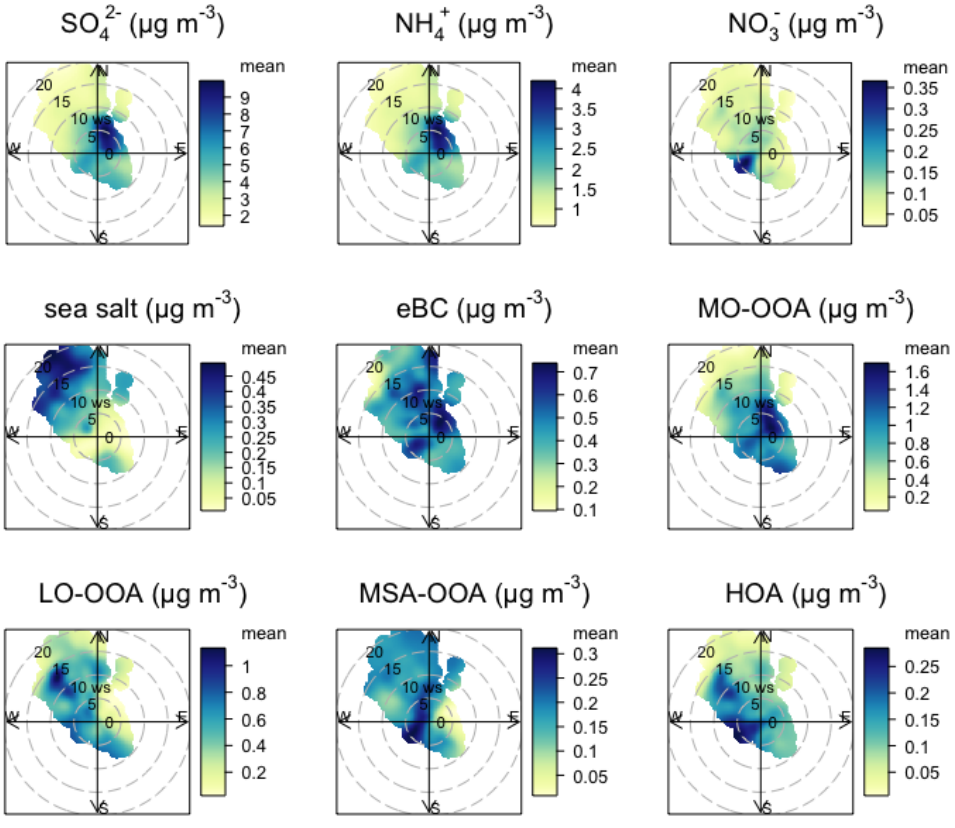

965
966 *Figure 9 Bi-variate polar plots of mean concentrations of PM_1 species and f_{44} at Lampedusa. The angle represents the arrival*
967 *wind direction, the radius represents the wind speed and the colours represent the mean concentrations for the respective*
968 *wind directions and winds.*

Atmos. Chem. Phys. Discuss., https://doi.org/10.5194/acp-2019-192
Manuscript under review for journal Atmos. Chem. Phys.
Discussion started: 12 March 2019

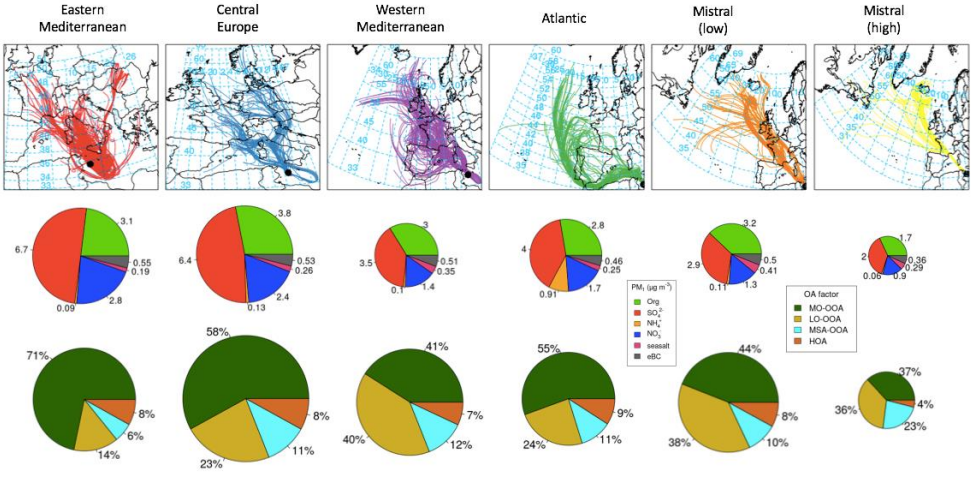

Figure 10 top) 144 hour air mass back trajectories, assigned to each cluster; middle) the PM_1 composition for each air mass cluster and bottom) the contribution of OA factors for each air mass cluster. The diameter for the PM_1 composition pie graphs are proportional to the total PM_1 concentration for each air mass cluster period and the radius for the OA factor pie graphs is proportional to the total PM_1 organic concentration for each air mass cluster period.

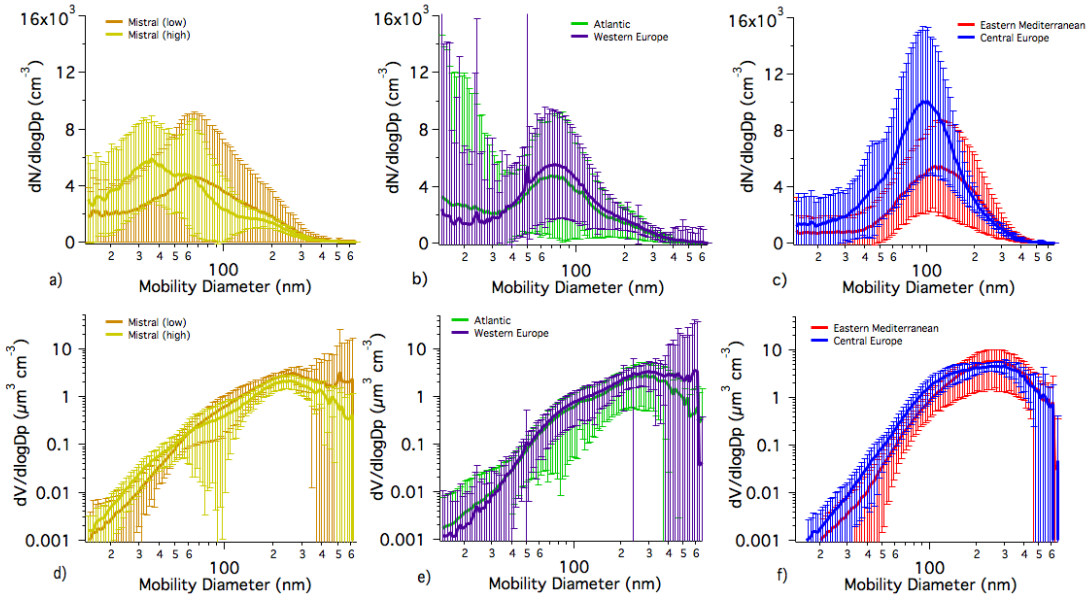

Figure 11 The number size distribution of PM_1 aerosol, coloured by averages for different air mass origin: a) Mistral (high) and Mistral (low); b) Atlantic and Western Europe; c) Eastern Mediterranean and Central Europe and the volume size distribution of PM_1 aerosol, coloured by averages for different air mass origin: d) Mistral (high) and Mistral (low); e) Atlantic and Western Europe; f) Eastern Mediterranean and Central Europe.

Atmos. Chem. Phys. Discuss., https://doi.org/10.5194/acp-2019-192
Manuscript under review for journal Atmos. Chem. Phys.
Discussion started: 12 March 2019

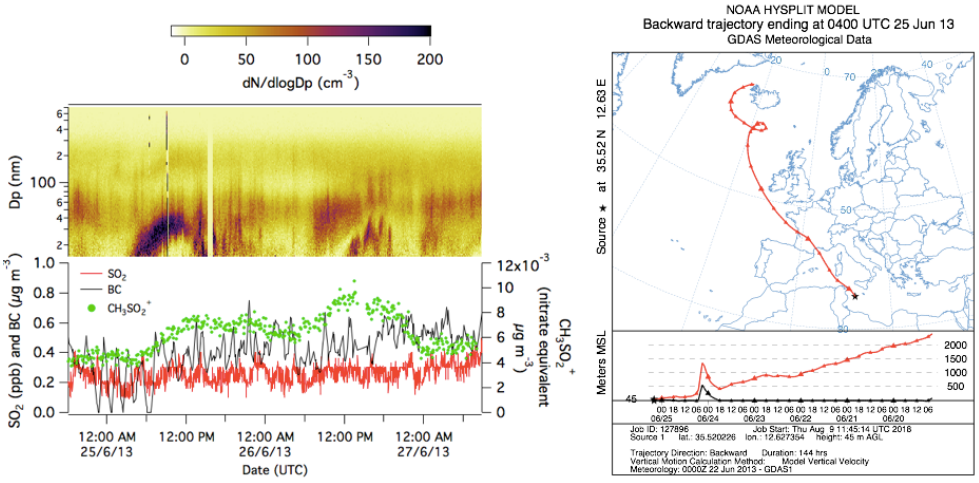

Figure 12 (left) The number size distribution during a new particle formation event on 25 June 2013 and the corresponding concentrations of SO_2, eBC and MSA fragment, $CH_3SO_2^+$, and (right) the HYSPLIT air mass backwards trajectory during the event.

Table 2 Campaign average PM_1 concentration for the major aerosol species measured at the Ersa and Lampedusa sites during the SOP-1a period and for periods of coincident air mass backwards trajectories between Ersa and Lampedusa

SITE	SO_4^{2-}	ORGANIC	NH_4^+	NO_3^-
ERSA	1.4 ± 2.6	3.0 ± 1.1	0.7 ± 1	0.3 ± 0.1
LAMPEDUSA	4.5 ± 0.9	3.0 ± 1.6	1.9 ± 0.5	0.1 ± 0.2
ERSA (COINCIDENT WITH LAMPEDUSA)	0.9 ± 0.5	2.7 ± 1.1	0.5 ± 0.3	0.4 ± 0.3
LAMPEDUSA (COINCIDENT WITH ERSA)	5.3 ± 2.0	3.8 ± 0.8	2.0 ± 0.6	0.1 ± 0.1

Atmos. Chem. Phys. Discuss., https://doi.org/10.5194/acp-2019-192
Manuscript under review for journal Atmos. Chem. Phys.
Discussion started: 12 March 2019

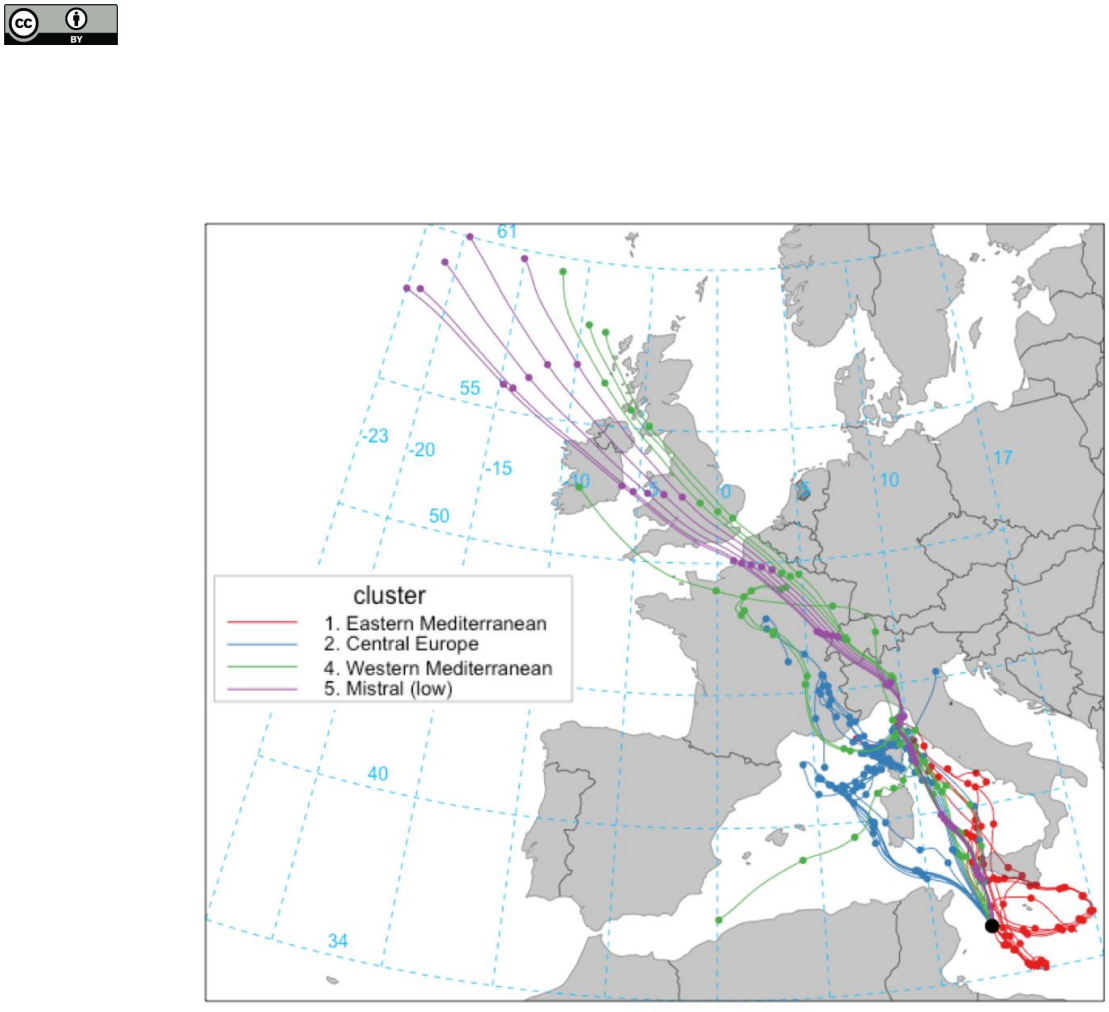

986

987 *Figure 13 Hourly 120-hour (5 days) backwards trajectories from Lampedusa that passed within ±1° in latitude and longitude*
988 *and ±200 m in altitude of the Ersa station. The colours represent the assigned cluster (performed on 144 hour trajectories).*

989

Atmos. Chem. Phys. Discuss., https://doi.org/10.5194/acp-2019-192
Manuscript under review for journal Atmos. Chem. Phys.
Discussion started: 12 March 2019

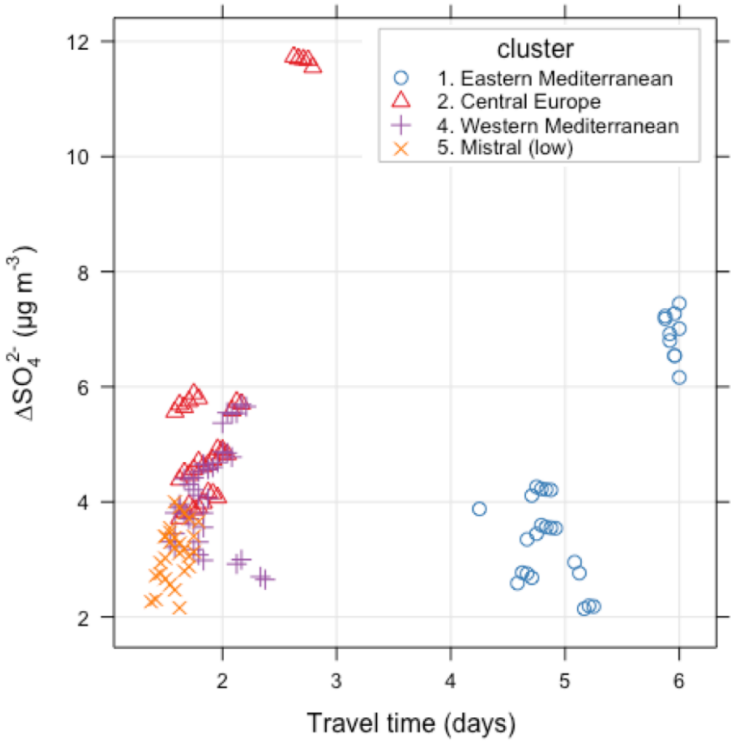

990

991 *Figure 14 The difference in the PM_1 SO_4^{2-} mass concentration at Lampedusa and Ersa as a function of the travel time of the*
992 *air masses from Ersa to Lampedusa. Colours represent the air mass origin cluster.*

993